AD NUMBER: AD0832600
LIMITATION CHANGES
TO: Approved for public release; distribution is unlimited.
FROM: Tnis document is subject to special export controls and each transmittal to foreign nationals or foreign govermnents may be made only with prior approval of AFWL (WLDE), Kirtland AFB, NM, 87117. Distribution is limited because of the technology discussed in the report.
AUTHORITY
ST-A AFWL LTR, 30 NOV 1971

AFWL-TR-
67-147

AN ANALYSIS OF TRANSMITTED SIGNAL DISTORTION RESULTING FROM ANTENNA TO REFLECTING SURFACE VELOCITY

J. Philip Castillo

TECHNICAL REPORT NO. AFWL-TR-67-147

May 1968

AIR FORCE WEAPONS LABORATORY
Air Force Systems Command
Kirtland Air Force Base
New Mexico

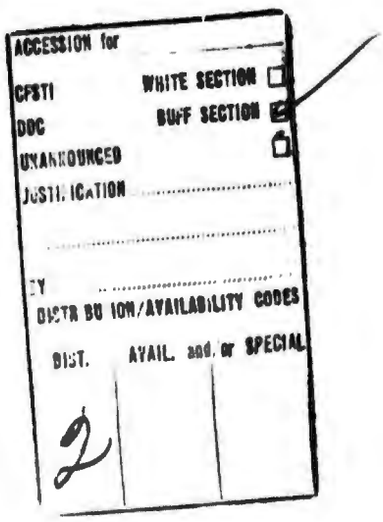

AIR FORCE WEAPONS LABORATORY
Air Force Systems Command
Kirtland Air Force Base
New Mexico

AN ANALYSIS OF TRANSMITTED SIGNAL DISTORTION RESULTING FROM ANTENNA TO REFLECTING SURFACE VELOCITY

J. Philip Castillo

TECHNICAL REPORT NO. AFWL-TR-67-147

FOREWORD

This research was performed under Program Element 6.24.05.06.F, Project 5791, Task 30.

Inclusive dates of research were September 1966 to February 1967. The report was submitted 13 December 1967 by the Air Force Weapons Laboratory Project Officer, Mr. J. Philip Castillo (WLDE).

The author wishes to express his appreciation to Dr. Arnold Koschmann, Chairman of the Electrical Engineering Department, University of New Mexico, for his many helpful suggestions during preparation of this report.

This technical report has been reviewed and is approved.

J. PHILIP CASTILLO
Project Officer

PARLEY D. CRONQUIST
Major, USAF
Chief, Electronics Branch

GEORGE C. DARBY, JR.
Colonel, USAF
Chief, Development Division

ABSTRACT

(Distribution Limitation Statement No. 2)

Distortion of transmitted signals caused by Doppler frequency spreading and amplitude modulation is a consequence of the relative velocity between the transmitter and a reflecting surface. General equations yielding velocity components to any point in the illuminated area on the surface, received power as a function of time, and generalized effects of vehicle motion on the transmitted frequency spectrum are derived. The Fourier spectrum of the range modulation function is calculated using computer techniques. With this, the spectral spreading of the transmitted signal due to rate of change of range is obtained. A specific transmitting-receiving system is analyzed. The system transmits a frequency-modulated continuous-wave (FM-CW) signal. The receiver consists of a balanced mixer, a band-pass filter, a square-law device, and a low-pass filter. The analysis of the system begins with the signal received from a single point reflector and is extended to signals received from many points simultaneously. This particular system is selected because it allows a unique analysis, in that the functional design would be dependent on the amount of signal distortion as defined in this research. A summary of the analysis is given, together with recommendations of topics for further study in the area of analysis of signals returned from various terrains.

CONTENTS

CONTENTS (cont'd)

ILLUSTRATIONS

ILLUSTRATIONS (cont'd)

SECTION I

INTRODUCTION

The distortion of a transmitted signal caused by Doppler frequency spreading and amplitude modulation is a consequence of the relative velocity between the transmitter and a reflecting surface.

The Doppler effect is associated with the apparent compression, or lengthening of the transmitted signal wavelength, resulting from a positive or negative relative velocity between a transmitter and receiver. One of the problems will be the determination of the degree of frequency spreading caused by a finite antenna beamwidth as the transmitter approaches a reflecting surface at a constant velocity. We shall show that the Doppler spreading is a function of antenna beamwidth.

The radar equation permits the determination of received power as a function of range, radar cross section, and the radar system parameters. Because the transmitter is moving toward the reflecting surface at a constant rate, the received signal amplitude will be continuously increasing as dictated by the radar equation; thus, the received signal is increasing as a function of time and will be in the form of an amplitude modulated signal. This amplitude modulation presents a further spreading of the transmitted signal. Here, we shall show that the spectrum spreading is a function of velocity and final altitude.

We shall first be interested in the properties of a signal reflected from a point target. A point target is physically impossible, but its concept will allow the formulation of relationships yielding velocity components to any point on the reflecting surface and received amplitude as a function of range. Having described the received signal in terms of a single point target, we shall then extend the analysis to a more complex target, namely, a thin reflecting strip directly below the transmitter.

A vehicle carrying both transmitter and receiver will be assumed to have started transmitting the signal at a distance h_o from the reflecting surface. It will then travel at a constant velocity V toward the surface. Because the

radar equation remains valid only for distances exceeding the near-field* of the transmitted electromagnetic energy, the analysis will not be carried out in this region. Numerically we shall show the degree of expected Doppler and spectrum spreading for various values of velocity, vehicle path angle,** and antenna beamwidth. We shall also vary the value of the final vehicle distance from the reflecting surface.

By using the results of the analysis, we shall then determine the effects of the spectrum spreading on an FM-CW system consisting of a transmitter and a receiver. The receiver will be made up of a mixer, a bandpass filter, a square-law device, and a low-pass filter. This particular receiver is selected because it allows a unique analysis in that the functional design would be dependent on the amount of signal distortion as defined in this report.

The problem of reflection of electromagnetic energy from terrain has been studied extensively (Refs. 1, 2, and 3). The problem, in general, has been to determine the effects of a random reflecting surface on a transmitted electromagnetic signal. Experimental data have been obtained in an effort to correlate the practical problem with the theory. In some cases, good agreement with the theory has resulted.

For a rough surface, a true vectorial analysis, based on electromagnetic theory, quickly becomes too complex because of the unknown boundary conditions at the random reflecting surface; consequently, several scalar models of reflecting surfaces have been proposed (Refs. 1, 2, 3, and 4). Moore (Ref. 5) has proposed an approximate solution by resolving the reflected signal into a specular (coherent) and a scattered (incoherent) return. In his report, Moore concludes that

> "...for a Gaussian distribution of heights from mean ground level, the relative contributions due to specular reflection and random scatter vary in accordance with

---

*The near-field is usually defined within a distance $2L^2/\lambda$ from the antenna, where L is the aperture length and λ is the wavelength of the transmitted signal.

**Path angle is here defined as the angle between a vehicle's flight path (assumed straight) and the horizontal.

> the negative exponential of the square of the ground standard deviation expressed in wavelengths."

Moore also concludes that "the fading of signals from the ground (due to the roughness) is the same statistically as the fluctuation of the amplitude of a signal in noise."

Davies (Ref. 2) proposes a technique with reflection and scattering of electromagnetic waves from slightly rough and very rough surfaces. Davies shows the results of an experimental program and its limited agreement with the theory. Davies also indicates that the reflected signal may be resolved into specular and scattered components.

Most of the models for a reflecting surface are a consequence of the Huygens principle (Ref. 6), i.e., each point in a plane wave can be considered as an individual source and the net result of the wave is the summation of the point sources. In this way, it is possible to assume that each incremental area on the reflecting surface contributes an incremental radar cross section, and the average effect of all incremental areas is caused by the average cross section.

In this study we shall use a scalar model for the signal analysis and assume the validity of summing signals contributed by small increments on the surface.

SECTION II

GEOMETRY OF TRANSMISSION

In this section, we shall define the geometry of the flight path and antenna beam with respect to the reflecting surface. A coordinate system will be selected such that the origin is located directly below the antenna, i.e., the line between the origin and the antenna is perpendicular to the reflecting surface. We shall also formulate a general transmitted and received signal.

1. Coordinate System

The location of the antenna, together with the antenna pattern and the reflecting surface, is shown in figure 1. We have selected a right-hand-coordinate system. The origin of the coordinate system is located directly below the transmitting antenna and moves along with the vehicle. The vehicle moves toward the reflecting surface in the y-z plane at a velocity V relative to the surface. The angle γ defines the flight path angle between the horizontal and the flight path. We shall assume that the antenna pattern forms a right circular cone defined by the altitude h, the vertex v, and the half angle β. In a later section we shall define an antenna gain equation.

To determine the return signal from any point within the antenna beam, we shall define a general point P within the beam on the surface. Rather than locating P by our Cartesian coordinate system, it will be simpler if we use the polar coordinates θ and ρ, i.e., $P = P(\theta,\rho)$. The range between the antenna at V and the point P will be denoted by the distance R.

2. Signal Considerations

Consider a signal transmitted to the incremental area ΔA_i located by the i^{th} point $P(\theta_i,\rho_i)$. The signal returned from ΔA_i is

$$S_{ri}(t) = K_i(t)\, S_t\left[t - \frac{2R_i(t)}{c}\right] \qquad (1)$$

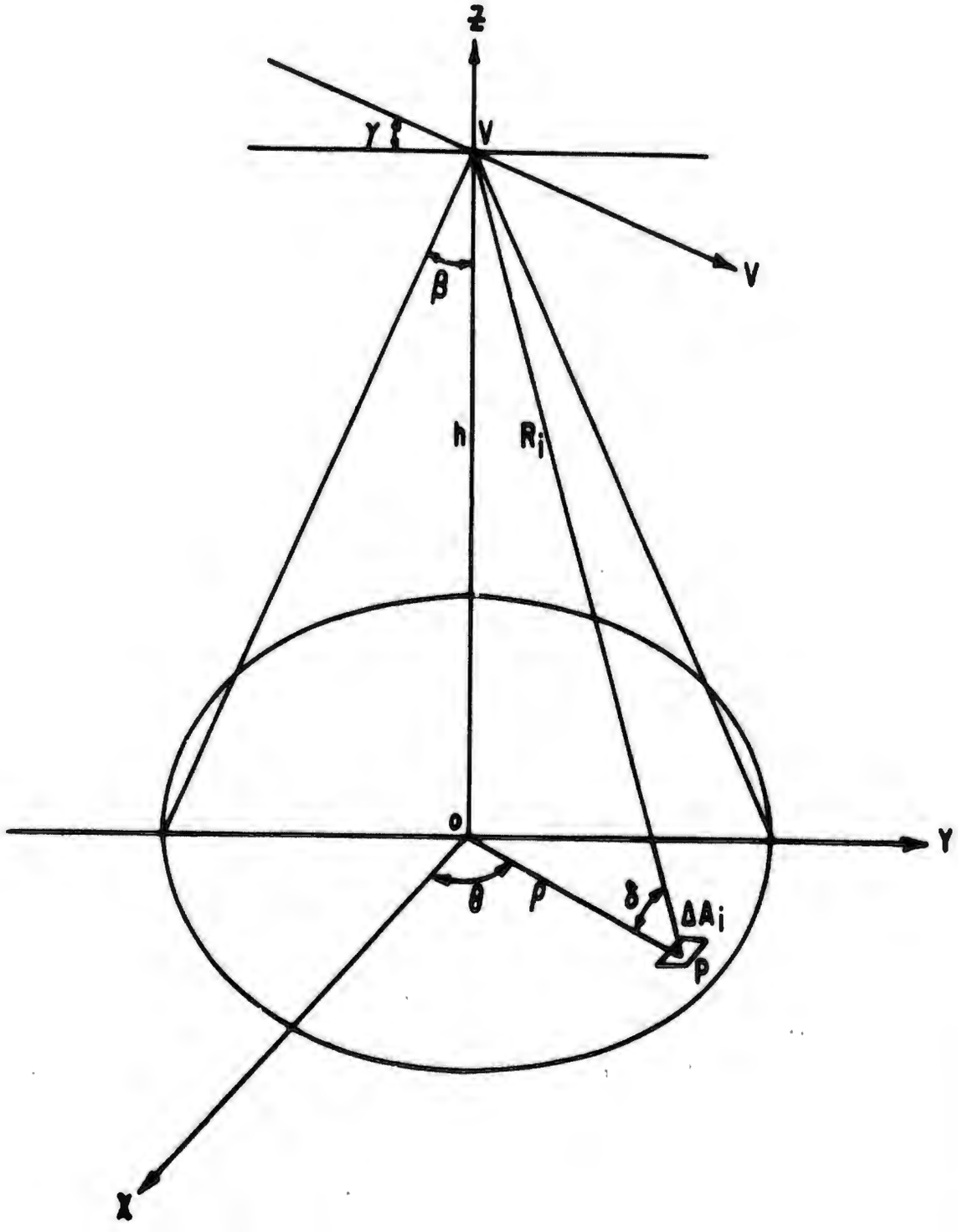

Figure 1. Antenna Geometry

where $K_i(t)$ is the attenuation of the transmitted signal as a function of time, S_t is the transmitted signal function, and c is the velocity of propagation. The range is given by

$$R_i(t) = R_{oi} - V_i t \tag{2}$$

where V_i is the velocity component to the i^{th} point and R_{oi} is the initial range. The total delay of the signal in propagating to and from the surface is given in equation (1) as

$$\frac{2R_i(t)}{c}$$

where we have assumed that $V_i \ll c$, where c is the velocity of propagation (see Appendix I). Because it is possible that the i^{th} point may be described by either a positive or a negative velocity component, we will write equation (2) as

$$R_i(t) = R_{oi} \pm V_i t \tag{3}$$

By substituting equation (3) into equation (1), we obtain

$$S_{ri}(t) = K_i(t)\, S_t\left[t - \frac{2R_{oi}}{c} \pm \frac{2V_i}{c}\, t\right] \tag{4}$$

For a stationary vehicle $V_i = 0$, and equation (4) becomes

$$S_{ri}(t) = K_i(t)\, S_t\left[t - \frac{2R_{oi}}{c}\right] \tag{5}$$

Comparing equations (4) and (5), we see that the effect of velocity is to introduce a "time compression" or "expansion," depending on whether the velocity component is positive or negative, respectively.

In Appendix I, we have derived an exact solution for the total transmission delay. Also, in Appendix I we have shown that the effect of velocity on a transmitted signal spectrum is to decrease the amplitude and stretch the spectrum by the factor

$$a = 1 + \frac{2V}{c}$$

The phase shift of the received signal with respect to the transmitted signal is found to be a linear function of frequency

$$\phi_r(\omega) = \frac{2R_o}{c}\omega$$

The velocity component to any point within the antenna pattern* is

$$V(\theta,\delta) = |V|(\sin\gamma \sin\delta + \cos\gamma \cos\delta \sin\theta)$$

where $|V|$ is the magnitude of the vehicle velocity along the flight path, γ is the path angle, δ is the angle of incidence, and θ is the azimuth angle on the surface (see figure 1). Of course, if we are given a particular transmitted frequency, the Doppler shift may be calculated from

$$\omega_d = \frac{2V}{c}\omega_c$$

where ω_c is the carrier frequency.

From the results of Appendix II, we may find the lines of constant Doppler on the surface; for example, if $\gamma = \pi/2$ (a vertical flight path), the velocity then becomes

$$V(\theta,\delta) = |V| \sin\delta \qquad (6)$$

and the lines of constant velocity on the surface become circles.

---

*See Appendix II for derivation.

3. The Total Received Signal

Equation (5) will allow us to determine the signal returned from a single increment on the surface. If we assume that the total signal from within the antenna beam on the surface is the sum of the contributions from all increments on the surface, we can write the received signal as

$$S_r(t) = \sum_{i=1}^{N} K_i(t)\, S_t\left[\left(1 \pm \frac{2V_i}{c}\right)t - \frac{2R_{oi}}{c}\right] \qquad (7)$$

where we are considering N increments.

In this section we have derived general equations for signals returned from a single point and N points; we have also defined a coordinate system. In the following section we shall formulate exact expressions for the return signal.

SECTION III

SIGNAL ANALYSIS

In this section, we shall determine the amplitude and phase of the return signal. We shall begin with the radar equation as a means of determining the return from a point on the surface and sum the return from all points to obtain the total return as seen at the receiving antenna. The amplitude of the received signal will be defined from the radar equation as the square root of the received power (across a 1-ohm resistor). We shall find that because of the continuously decreasing distance between the antenna and the target, the received signal amplitude will have the form of a double sideband modulated (DSB) signal.

As a result of the relative velocity between the antenna and the target, the carrier frequency will be shifted by a factor proportional to the relative velocity. Also, the time delay in propagating to and from the target will appear as a phase shift.

We shall combine the resulting amplitude and phase representations to obtain the effects of velocity and antenna beam width on the amplitude and phase of a transmitted signal.

1. Power Considerations

The power reflected from a smooth, flat, infinite surface and intercepted by the receiving antenna is determined by the radar equation

$$P_r = \frac{P_t G^2 \lambda^2 \rho_r G_s A_s \sin \delta}{(4\pi)^3 R^4} \tag{8}$$

where

P_r is the received power

P_t is the transmitted power

ρ_r is the power reflection coefficient

G_s is the scatterer gain in the direction of the source

A_s is the illuminated area

δ is the angle of incidence

R is the range from A_s to the source

G is the antenna gain

λ is the radio frequency wavelength

A backscattering cross section is given by reference 7

$$\sigma = \rho_r G_s A_s \sin \delta \tag{9}$$

and an average cross section per unit area by

$$\sigma_o = \rho_r G_s \tag{10}$$

From equation (10) and equation (8), the power received can be written as

$$P_r = \frac{P_t G^2 \lambda^2 \sigma_o \sin \delta A_s}{(4\pi)^3 R^4} \tag{11}$$

The power received from an element of area dA_s is

$$dP_r = \frac{P_t G^2 \lambda^2 \sigma_o \sin \delta \, dA_s}{(4\pi)^3 R^4} \tag{12}$$

The antenna gain G may be written as a function of angle of incidence (Ref. 8)

$$G(\delta) = G_o \sin^2 \delta \tag{13}$$

where G_o is the gain on the antenna axis. By substituting equation (13) into equation (11), we obtain

$$dP_r = \frac{P_t G_o^2 \lambda^2 \sigma_o \sin^5 \delta \, dA_s}{(4\pi)^3 R^4} \tag{14}$$

Normally, P_t (transmitted power), λ (wavelength), and G_o are constant. Assuming a constant average cross section over the illuminated area we can write

$$C = \frac{P_t G_o^2 \lambda \sigma_o}{(4\pi)^3} \tag{15}$$

then

$$dP_r = C \frac{\sin^5 \delta \, dA_s}{R^4} \tag{16}$$

The total received power from each element over the illuminated area may now be obtained by integrating equation (16):

$$P_r = C \int_{A_s} \frac{\sin^5 \delta \, dA_s}{R^4} \tag{17}$$

From figure 2, dA_s can be determined as

$$dA_s = \rho \, d\rho \, d\theta \tag{18}$$

but because

$$\rho^2 = R^2 - h^2 \text{ and } \sin \delta = \frac{h}{R} \tag{19}$$

we can write

$$dA_s = Rd \, Rd\theta \tag{20}$$

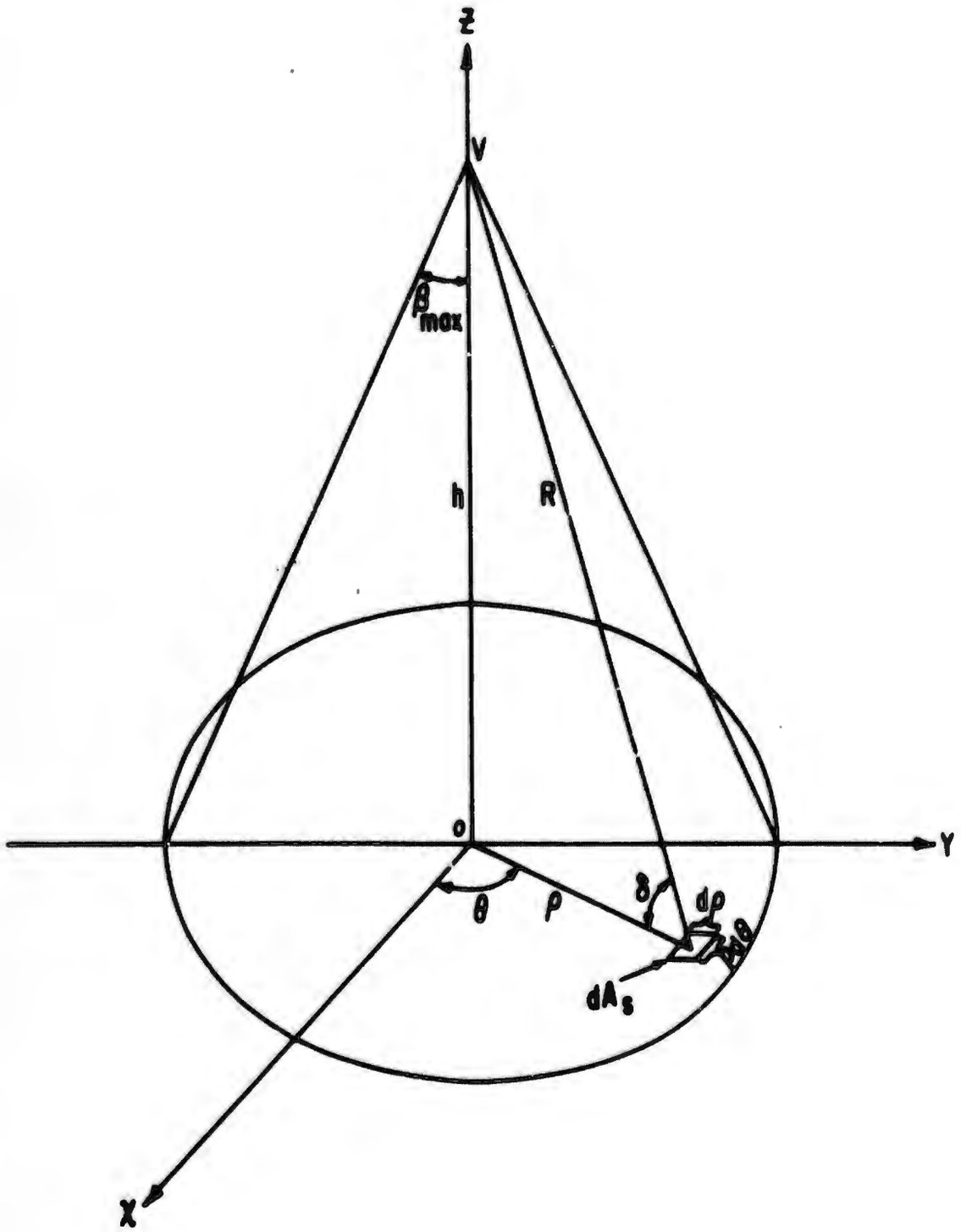

Figure 2. Geometry for Determining Power Returned from an Element of Illuminated Area

and

$$P_r = C \int_0^{2\pi} d\theta \int_h^{R_{max}} \frac{h^5 \, d\,R \, d\,\theta}{R^8} \tag{21}$$

By completing the integration, we obtain

$$P_r = \frac{2}{7} \pi \, Ch^5 \left[\frac{1}{h^7} - \frac{1}{R_{max}^7} \right] \tag{22}$$

The vertical altitude h may be written as a function of time, i.e.,

$$h(t) = h_o - V_z \, t \tag{23}$$

and the maximum range then becomes

$$R_{max} = \frac{h(t)}{\sin \delta_{min}} \tag{24}$$

where h_o is the initial altitude and V_z is the antenna vertical velocity component. By substituting equation (23) into equation (22), we obtain

$$P_r(t) = \frac{2}{7} \pi \, C \, \frac{1 - \sin^7 \delta_{min}}{\left(h_o - V_z t\right)^2} \tag{25}$$

or, in terms of the antenna beam width,

$$P_r(t) = \frac{2}{7} \pi \, C \, \frac{1 - \cos^7 \beta_{max}}{\left(h_o - V_z t\right)^2} \tag{26}$$

where β_{max} is defined in figure 2 and is a constant.

The original assumption of C = constant will now be discussed. C was given by equation (15)

$$C = \frac{P_t G_o^2 \lambda^2 \sigma_o}{(4\pi)^3}$$

There is no problem in assuming that

$$\frac{P_t G_o^2 \lambda^2}{(4\pi)^3} = \text{constant}$$

because these parameters can be controlled during the system design stages. We must focus our attention on the average cross section σ_o. As has already been shown (equation (10)), for a smooth, infinite, flat surface

$$\sigma_o = \rho_r G_s$$

where ρ_r is the power reflection coefficient and G_s is the scatterer gain in the direction of the source. For an isotropic and homogeneous surface, ρ_r will remain constant and will be independent of geometrical considerations. The scatterer gain, G_s, is determined (at the receiver) by the vector sum of the field components from contributions of all incremental areas on the surface and it is clear that, for our problem of a flat, infinite surface, G_s will be independent of position over the surface and consequently, will be constant. In a practical problem where the reflecting surface is random, G_s will be a function of position (Ref. 2). The quantity, σ_o, is usually determined experimentally (Refs. 1, 2, and 4).

2. Derivation of the Return Signal

We have determined expressions for velocity to any point on the surface and the total reflected power. We have also determined an expression for the return signal as modified by vehicle motion. Here we shall formulate an expression for the total signal.

The expression for the velocity component to any point on the surface due to vehicle motion has been found to be (Appendix II)

$$V(\theta,\delta) = |V| \ (\sin \gamma \sin \delta + \cos \gamma \cos \delta \sin \theta)$$

which is a function of azimuth angle θ, angle of incidence δ, and path angle γ. The path angle is assumed constant for a particular problem. This expression for velocity is important in the present analysis and in the final model since it becomes a factor in the determination of rate of change of received power and total Doppler shift.

The total power from the illuminated circle on the reflecting surface as a function of time was found to be (equation (26))

$$P_r(t) = \frac{2}{7} \pi C \frac{1 - \cos^7 \beta_{max}}{\left(h_o - V_z t\right)^2}$$

where

$$C = \frac{P_t G_o^2 \lambda^2 \sigma_o}{(4\pi)^3} = \text{constant}$$

$P_r(t)$ was derived by assuming that the antenna gain as a function of angle of incidence δ is (equation (13))

$$G = G_o \sin^2 \delta$$

The return power is a maximum when β, the beam angle, is $\pi/2$, and approaches zero when β approaches zero. The analysis of return power is not as simple as indicated, since, as β approaches $\pi/2$, the angle of incidence δ approaches zero and the antenna gain approaches zero.

Because the return power, as derived, involves total power, the expression is not valid if we assume a varying cross section σ_o over the illuminated area. It is desirable to obtain an expression for return power from an

elemental area for which σ_o can be assumed to be constant and sum all the power returned from the illuminated area as a function of σ_o. In a practical problem, σ_o is a random quantity and a particular probability density will have to be assumed (or measured), depending on the surface characteristics.

Kerr (Ref. 6) defines σ as "the area intercepting that amount of power which, when scattered isotropically, produces an echo equal to that observed from the target."

Consider an element of area ΔA_s as shown in figure 3. This elemental area is selected such that the angles θ and δ remain constant as the vehicle moves toward the surface. The vertical altitude is given by

$$h(t) = h_o - V_z t$$

where h_o is the initial altitude and V_z is the vertical velocity. The range to ΔA_s is given by

$$R(t) = \frac{h(t)}{\sin \delta} = h(t) \csc \delta \tag{27}$$

For an isotropic scatterer, ΔA_s, the power returned to the source as a function of time, is

$$\Delta P_r(t) = \frac{P_t G^2 \lambda^2 \sin \delta \, \Delta A_s}{(4\pi)^3 [R(t)]^4} \tag{28}$$

The antenna gain has been assumed to be

$$G = G_o \sin^2 \delta$$

where G_o is the maximum gain along the vertical axis. By substituting into equation (28), we obtain

$$\Delta P_r(t) = \frac{P_t G_o^2 \lambda^2 \sin^5 \delta \, \Delta A_s}{(4\pi)^3 [R(t)]^4} \tag{29}$$

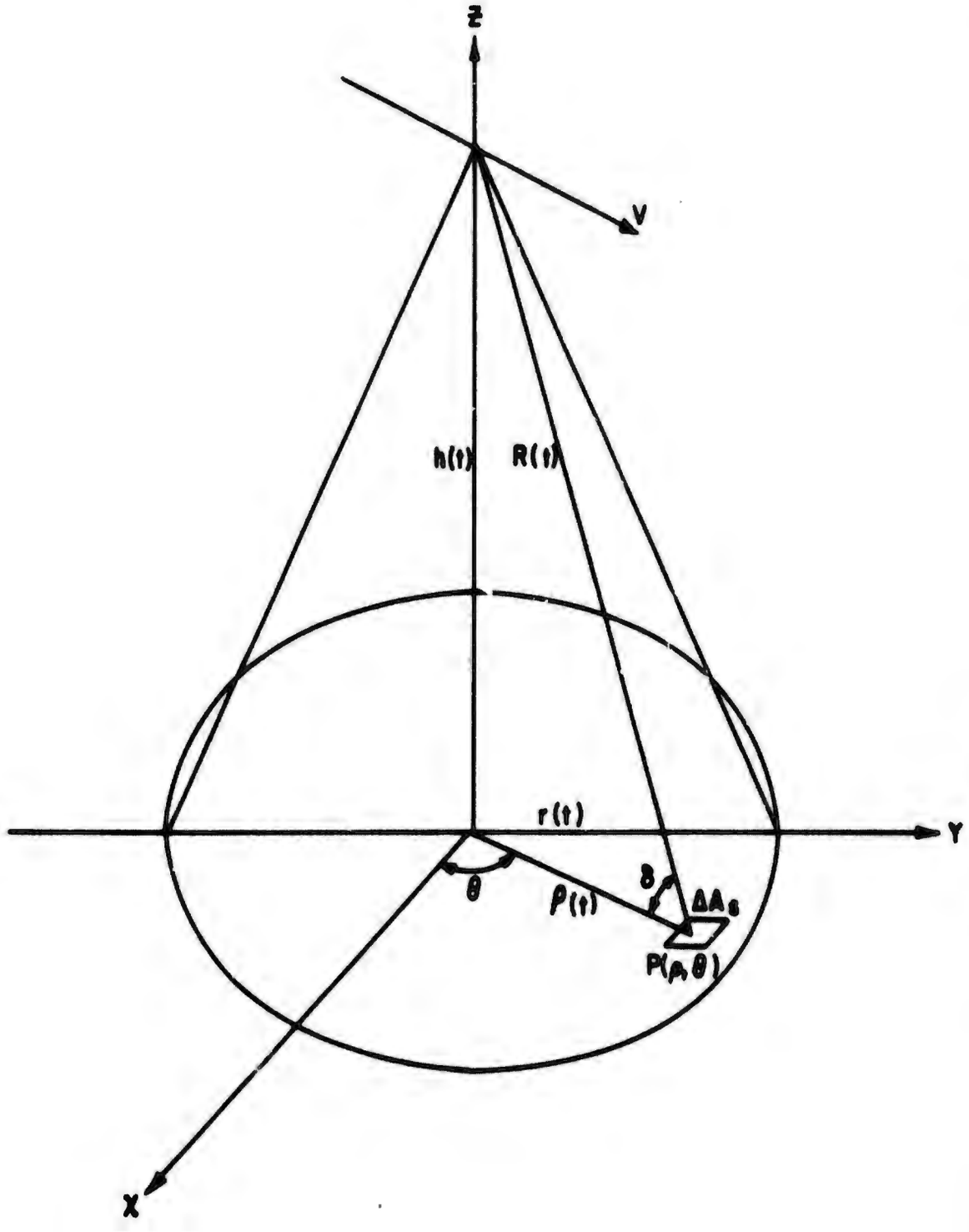

Figure 3. Scattering Element ΔA_s

or because

$$\frac{P_t G_o^2 \lambda^2}{(4\pi)^3} = C = \text{constant}$$

$$\Delta P_r(t) = C \frac{\sin^5 \delta}{[R(t)]^4} \Delta A_s \tag{30}$$

For a smooth, homogeneous, isotropic, infinite surface the characteristics of ΔA_s will not vary as it moves over the surface, although in practical problems the properties of ΔA_s may vary considerably. In fact, the power reflection coefficient ρ_r and the scatterer gain G_s may vary rapidly such as over snow surfaces or across paved roads. In a practical problem the properties of the area ΔA_s are usually considered to vary randomly (Refs. 2 and 4).

For a transmitted signal $S_t(t)$, the received signal was found to be

$$S_r(t) = K(t)\, S_t \left[t\left(1 + \frac{2V(\theta,\delta)}{c}\right) - \frac{2R_o}{c} \right] \tag{31}$$

where K(t) is the attenuation factor and is defined as (see equation (29))

$$K(t) = \left[\frac{\Delta P_r(t)}{P_t}\right]^{1/2} = \left[\left(\frac{G_o^2 \lambda^2}{(4\pi)^3}\right)\left(\frac{\sin^5 \delta\, \Delta A_s}{[R(t)]^4}\right)\right]^{1/2} \tag{32}$$

Then the received signal can be written as

$$S_r(t) = K \frac{\left[\sin^5 \delta\, \Delta A_s\right]^{1/2}}{[R(t)]^2} S_t \left[t\left(1 + \frac{2V(\theta,\delta)}{c}\right) - \frac{2R_o}{c} \right] \tag{33}$$

where

$$K = \frac{G_o \lambda}{(4\pi)^{3/2}}$$

If we recall that the range R_o is an arbitrary initial range, then we can define the relation

$$\sin \delta = \frac{R_o}{h_o}$$

between the initial range and the initial vertical altitude; as δ approaches $\pi/2$, R_o approaches h_o.

Equation (33) may be written as

$$S_r(t) = K \frac{\left[\sin^5 \delta \, \Delta A_s\right]^{1/2}}{[R(t)]^2} S_t[t - \tau(t)] \qquad (34)$$

where $\tau(t)$ is the total time of propagation to and from the target.

$$\tau(t) = \frac{2R_o}{c} - \frac{2V(\theta,\delta)}{c} t \qquad (35)$$

The delay (equation (35)) is a function of time and is continuously decreasing.

From equation (34), we can see that the received signal amplitude varies directly as

$$(\sin^{5/2} \delta)\left(\Delta A_s\right)^{1/2}$$

and inversely as

$$[R(t)]^2 = \left[\frac{h_o - V_z t}{\sin \delta}\right]^2 \qquad (36)$$

and the received amplitude may be written as

$$A(t) = K \frac{\sin^{9/2} \delta \left(\Delta A_s\right)^{1/2}}{\left(h_o - V_z t\right)^2} \tag{37}$$

because

$$R(t) = \frac{h_o - V_z t}{\sin \delta}$$

With equation (37), equation (36) may now be rewritten in general as

$$S_r(t) = A(t) \left[t - \tau(t)\right] \tag{38}$$

Equations (35), (37), and (38) define the signal returned from an incremental area within the illuminated surface. To obtain the total return at the receiving antenna, the contributions from all increments on the illuminated surface must be summed.

$$\left[S_r(t)\right]_{TOTAL} = \sum_{i=1}^{N} A_i(t) \, S_t\left[t - \tau_i(t)\right] \tag{39}$$

where the return from the i^{th} increment is (see equation (38))

$$S_{ri}(t) = A_i(t) \, S_t\left[t - \tau_i(t)\right] \tag{40}$$

In the next section the signal from a point target will be analyzed with respect to spectrum spreading and amplitude modulation.

SECTION IV

ANALYSIS OF A SIGNAL RETURNED FROM A POINT TARGET

So far we have discussed the effects of vehicle velocity, relative to the reflecting surface, on a transmitted signal. First, we have found that, because of a finite radiation beam width (Appendix II), a band of Doppler frequencies will be generated. Second, the radar equation shows that, due to a decreasing range as a function of time, the signal is continuously increasing, thus producing an amplitude modulation on the transmitted signal.

In this section, we shall summarize the effect of a continuously changing range on a transmitted signal as it is reflected from a point targer. From this we can extend our analysis to a signal returned from an extended target.

Consider a simple sinusoidal signal

$$S_t(t) = A_o \cos\left(\omega_o t + \phi\right) \tag{41}$$

transmitted toward the point target.

From equation (38), the return signal will then be

$$S_r(t) = A(t) \cos \omega_o \left[\left[t - \tau(t)\right] + \phi\right] \tag{42}$$

where

$$A(t) = \left\{\left(\frac{G_o^2 \lambda^2}{(4\pi)^3}\right)^{1/2} \frac{\sin^9 \delta \, \Delta A_s}{\left(h_o - V_z t\right)^4}\right\} \tag{43}$$

as in equation (37) and ϕ is the phase. If we select a point target where $\delta = \pi/2$, then equation (43) becomes

$$A(t) = \left(\frac{G_o \lambda}{(4\pi)^{3/2}}\right)\left(\frac{\left(\Delta A_s\right)^{1/2}}{\left(h_o - V_z t\right)^2}\right) \tag{44}$$

Let us normalize A(t) as follows:

$$A_n(t) = A(t) \left(\frac{(4\pi)^{3/2}}{G_o \lambda \left(\Delta A_s\right)^{1/2}} \right) = \frac{(\sin \delta)^{9/2}}{\left(h_o - V_z t\right)^2} \tag{45}$$

Then for our point target at $\delta = \pi/2$, we obtain

$$S_r(t) = A_n(t) \cos \left\{ \omega_o \left[t - \tau(t) \right] + \phi \right\} \tag{46}$$

Because ϕ is arbitrary, we can select $\phi = 0$ without loss of generality, and

$$S_r(t) = A_n(t) \cos \omega_o \left[t - \tau(t) \right] \tag{47}$$

From equation (35), we can write

$$\tau(t) = t_o - \lambda t \tag{48}$$

where

$$t_o = \frac{2R_o}{c}$$

and

$$\lambda = \frac{2V}{c}$$

Substitution of equation (48) into equation (47) yields

$$S_r(t) = A_n(t) \cos \omega_o \left(t - t_o + \lambda t \right)$$

or

$$S_r(t) = A_n(t) \cos \left[\left(\omega_o + \lambda \omega_o \right) t - \omega_o t_o \right] \tag{49}$$

Equation (49) has the form of a double-side-band (DSB) modulated signal shifted in frequency by the Doppler $\lambda\omega_o$ and shifted in phase by $\omega_o t_o$.

Frequency Analysis of $S_r(t)$

The fourier Transform of equation (49) is

$$S_r(\omega) = 1/2 \left\{ e^{-j\omega_o t_o} A\left[\left(\omega - \omega_o - \lambda\omega_o\right)\right] + e^{+j\omega_o t_o} A\left[\left(\omega + \omega_o + \lambda\omega_o\right)\right] \right\} \quad (50)$$

Equation (50) is the spectrum of the modulating range function $A_n(t)$ shifted symmetrically about the origin by $\left(\omega_o + \lambda\omega_o\right)$ with a constant phase shift $\omega_o t_o$. The amplitude spectrum is shown in figure 4.

Figure 4 shows the transmitted signal spread caused by the range modulation and the frequency shift due to Doppler effect. The return from any other point on the surface will be similar to figure 4 except for a different Doppler shift and amplitude. In the next section, we shall superimpose the returns from many points such as shown in figure 4 and we shall determine the degree of spreading due to the range function A(t) and the complete Doppler shift.

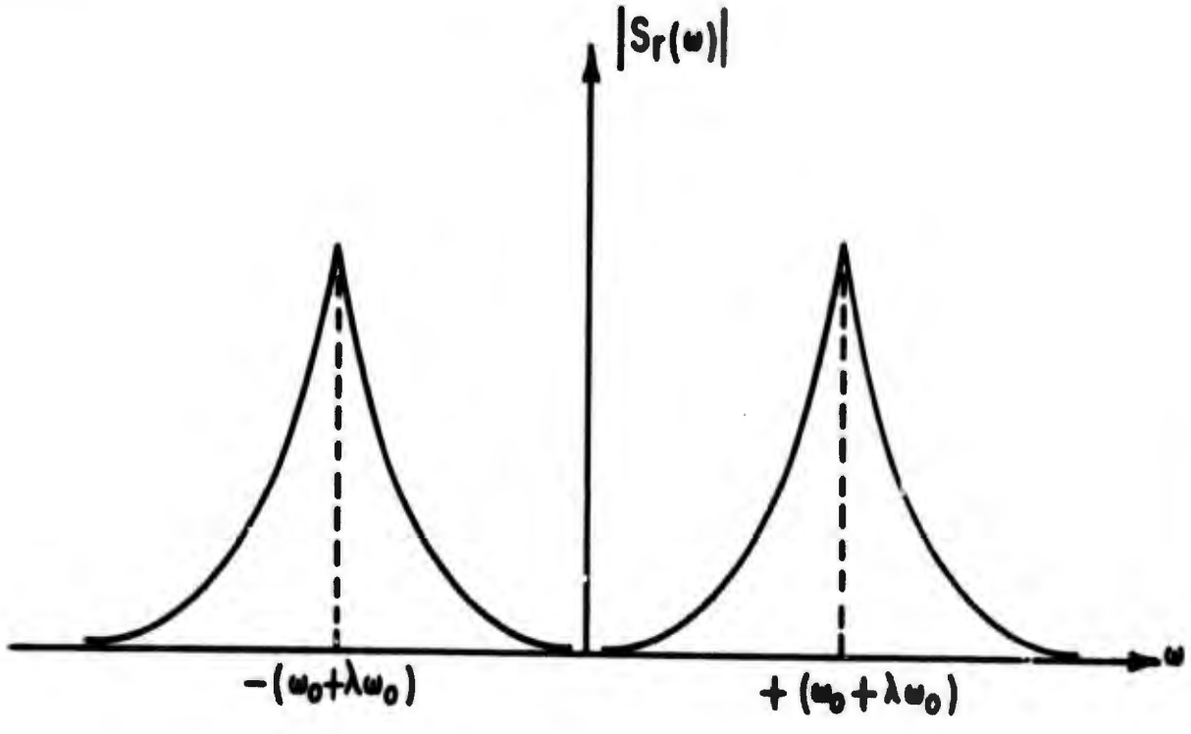

Figure 4. $S_r(t)$ Amplitude Spectrum

SECTION V

ANALYSIS OF A SIGNAL RETURNED FROM A THIN STRIP

In this section, we shall extend the analysis of the return signal from a point target to the signal returned from a thin strip of finite length. We assume that superposition holds and simply sum the signals returned from many points on the thin strip in order to obtain the net resultant signal.

We shall select the thin strip on the y-axis (see figure 3) such that the angle θ is either $+\pi/2$ or $-\pi/2$. We shall limit the analysis to the signal returned from N points. The received signal then becomes

$$S_r(t) = \sum_{i=1}^{N} A_{ni}(t) \cos\left[\left(\omega_o + \lambda_i\right) t - \omega_o t_o\right] \tag{51}$$

where

$$A_{ni}(t) = \frac{\left[\sin \delta_i\right]^{9/2}}{\left(h_o - V_z t\right)^2} \tag{52}$$

and

$$\lambda_i = \frac{2V_i}{c} \tag{53}$$

From equation (52), we can see that the maximum return occurs when $\delta = \pi/2$ as selected in the previous section, for $\delta \neq \pi/2$, $\sin \delta < 1$ and the return from other than the vertical ($\delta = \pi/2$) point decreases as δ decreases.

The Doppler shift is determined by the velocity components to the points on the thin strip (equation (53)). The velocity component to any point on the thin strip is given by

$$V_i = |V|\left(\sin\gamma \sin\delta_i + \cos\gamma \cos\delta_i\right)$$

$$= |V| \cos\left(\gamma - \delta_i\right) \text{ for } \theta = +\pi/2 \tag{54}$$

and

$$V_i = |V|\left(\sin\gamma \sin\delta_i - \cos\gamma \cos\delta_i\right)$$

$$= |V|\left[-\cos\left(\gamma + \delta_i\right)\right] \text{ for } \theta = -\pi/2 \tag{55}$$

From equations (54) and (55), the following properties of the velocity components are obtained:

$$V\left(\theta,\delta_i\right) \begin{cases} > 0 \text{ if } |\gamma - \delta_i| < \pi/2 \\ = 0 \text{ if } |\gamma - \delta_i| = \pi/2 \\ < 0 \text{ if } |\gamma - \delta_i| > \pi/2 \end{cases} \text{ for } \theta = +\pi/2 \tag{56}$$

$$V\left(\theta,\delta_i\right) \begin{cases} > 0 \text{ if } |\gamma + \delta_i| > \pi/2 \\ = 0 \text{ if } |\gamma + \delta_i| = \pi/2 \\ < 0 \text{ if } |\gamma + \delta_i| < \pi/2 \end{cases} \text{ for } \theta = -\pi/2 \tag{57}$$

Equations (56) and (57) indicate that under certain conditions the velocity component may become negative, thus yielding a negative Doppler shift. For example, say that

$$\gamma = \pi/6 \tag{58}$$

$$\delta_{min} = \pi/6 \tag{59}$$

$$\delta_{max} = \pi/2 \tag{60}$$

then, for $\theta = + \pi/2$

$$|\gamma - \delta_{min}| = 0 < \pi/2 \tag{61}$$

and

$$|\gamma - \delta_{max}| = \pi/3 < \pi/2 \tag{62}$$

By comparing equations (61) and (62) with (56), we see that the velocity components are positive for all δ when $\theta = + \pi/2$. For $\theta = - \pi/2$, we get

$$|\gamma + \delta_{min}| = \pi/3 < \pi/2 \tag{63}$$

$$|\gamma + \delta_{max}| = 3\pi/2 > \pi/2 \tag{64}$$

From equations (63), (64), and (57), the velocity components become positive for values of δ close to δ_{max}, and negative for values of δ close to δ_{min}. The point where the transition from positive velocity component to negative velocity component occurs when

$$|\gamma + \delta| = \pi/2$$

or

$$\delta = \pi/2 - \pi/6 = \pi/3$$

therefore,

$$\delta > \pi/3, \; V > 0$$

and

$$\delta < \pi/3, \; V < 0$$

Consider the signal returned from the thin strip shown in figure 5 with only 11 points being considered, then the spectrum due to the 11 points may appear as shown in figure 6, which shows the spectrum for $\omega > 0$. The total spectrum spreading is $\omega_o\left(\lambda_{11} - \lambda_1\right)$, assuming that the spreading caused by the range function A(t) is negligible compared to $\omega_o\left(\lambda_{11} - \lambda_1\right)$. The return caused by point six being directly beneath the transmitting antenna is seen to be the maximum contribution, while smaller contributions come from the outer points.

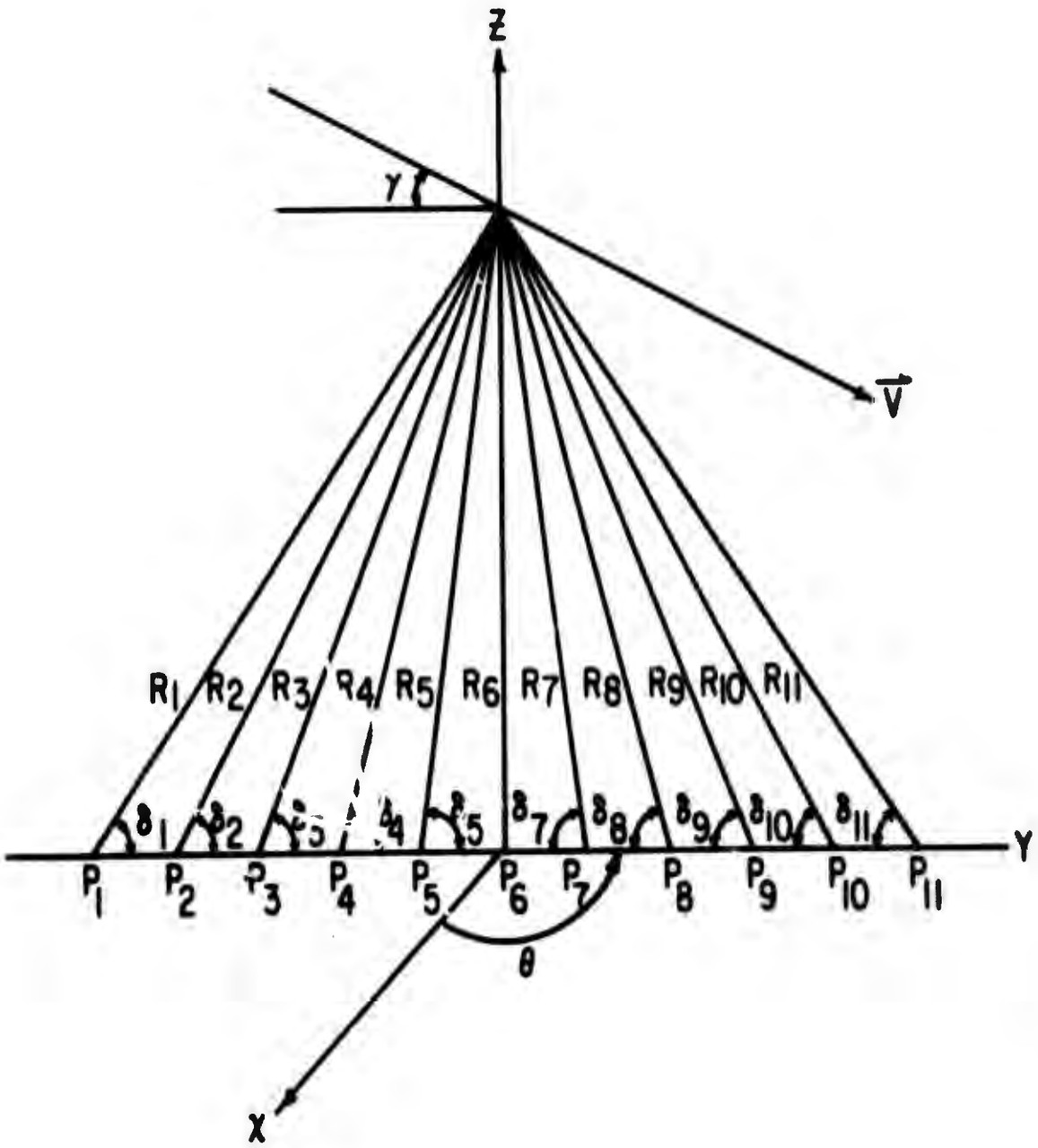

Figure 5. Return from a Thin Strip

Between the contributions, we have shown a slight overlap caused by neighboring points at the larger amplitude, which may or may not occur (see section VI). Intuitively, the degree of spreading caused by the range function A(t) is dependent on the velocity, V_z, i.e., the greater the velocity, the greater the spreading. In the next section, numerical calculations of the range amplitude spectrum will be made. We have mentioned the overlap between contributions of adjacent points only to point out the dependence of spreading on velocity. It is clear that the contributions from two adjacent points will always overlap if we choose the points close enough. If we consider the contributions from all points (an infinite number) on the thin strip, a continuous spectrum, as indicated by the dotted line in figure 6, will occur.

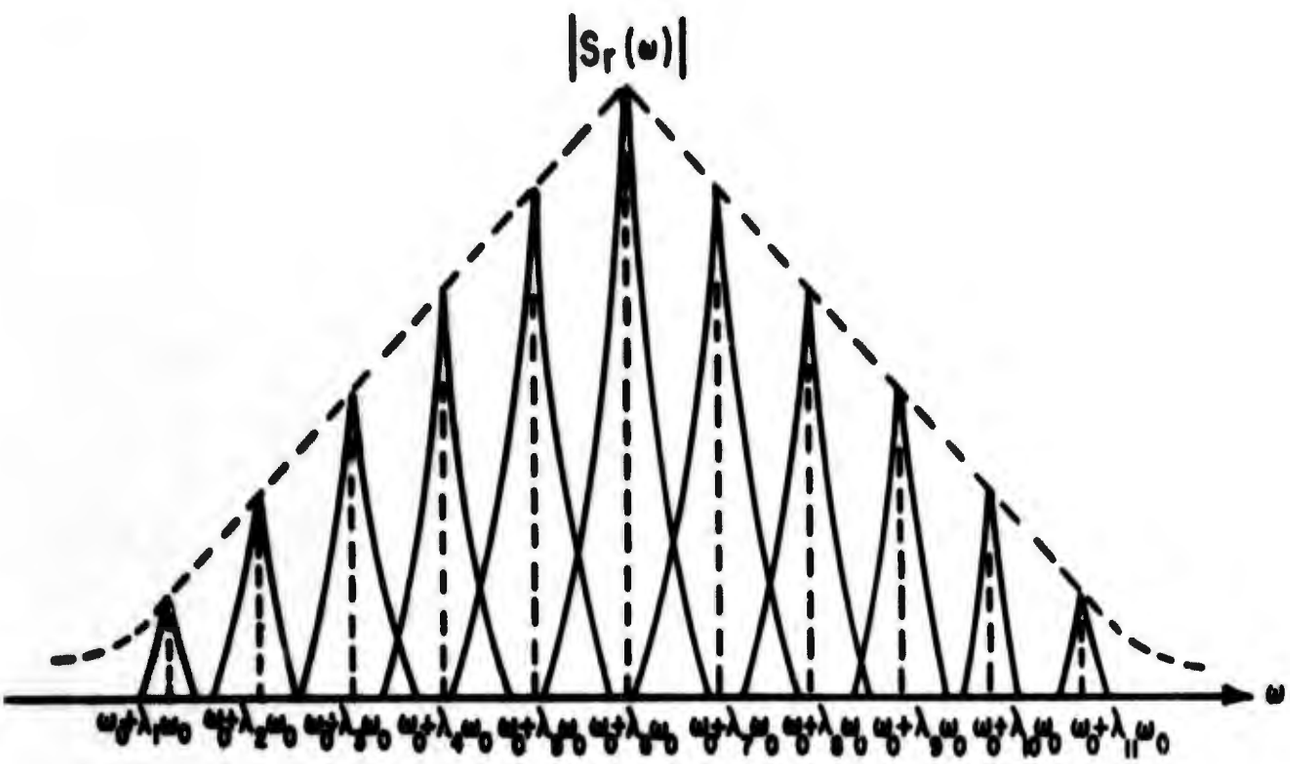

Figure 6. Amplitude Spectrum of Signal Received from a Thin Strip

In analyzing the return from all the illuminated area, we would want to consider returns from points of constant velocity. In general, the lines of constant velocity will be ellipsoidal (Appendix II) and the range to these points of constant velocity will vary and contributions to the total amplitude for a particular velocity will therefore vary with the angle θ and the return will not be symmetrical, as indicated in figure 6.

SECTION VI

NUMERICAL ANALYSIS OF A(t) AND DOPPLER SPREADING

In this section, the spread of the transmitted signal caused by velocity will be shown numerically for different values of velocity, flight path angle, antenna beam width, and final altitude. The dependence of signal spreading on the final antenna altitude has not yet been discussed. This phenomenon is caused by the rate of increase of the received signal which increases at a faster rate at the lower altitudes, thereby having the effect of spreading the transmitted signal more than at higher altitudes.

1. Amplitude as a Function of Time

Figure 7 shows the received amplitude,

$$A(t) = \frac{1}{\left(h_o - V_z t\right)^2}$$

as a function of time. Three different velocities are considered, 5×10^3 fps, 10×10^3 fps, and 15×10^3 fps. At time $t = 0$, the initial altitude is 10^5 feet and the final altitude is 500 feet. From the figure we can see that the amplitude increases by 4 orders of magnitude as the antenna moves from 10^5 feet to 500 feet. Intuitively, we can see that the received spectrum would be spread more for greater velocities. Also, because the rate of increase of the amplitude is greatest at the terminal altitudes, this would indicate that the smaller the terminal altitude, the greater the spectrum spreading.

2. A(t) Amplitude Spectrum

Figure 8 shows the A(t) amplitude spectrum for velocities of 5×10^3 fps, 10×10^3 fps, and 15×10^3 fps; $h_o = 10^5$ feet, and final altitude $h_f = 10^3$ feet. Here we can see that our previous assumption of greater spectrum spreading for greater velocities is verified. Figure 9 shows similar plots but for a final altitude of 10^2 feet. If we compare figures 8 and 9, we can see that the spectrum spreading increases rapidly for small terminal altitude (10^3 feet versus 10^2 feet).

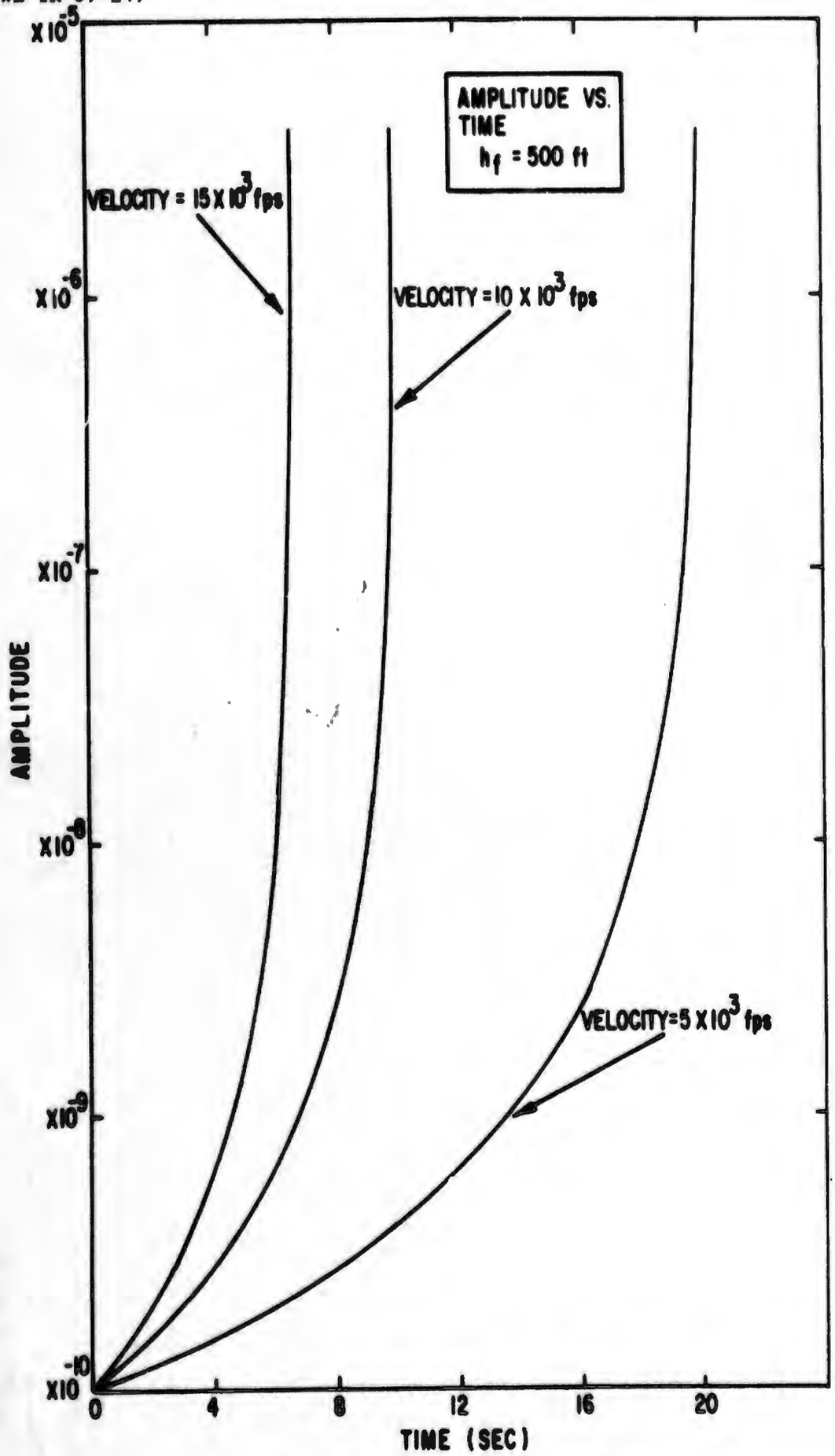

Figure 7. Amplitude as a Function of Time

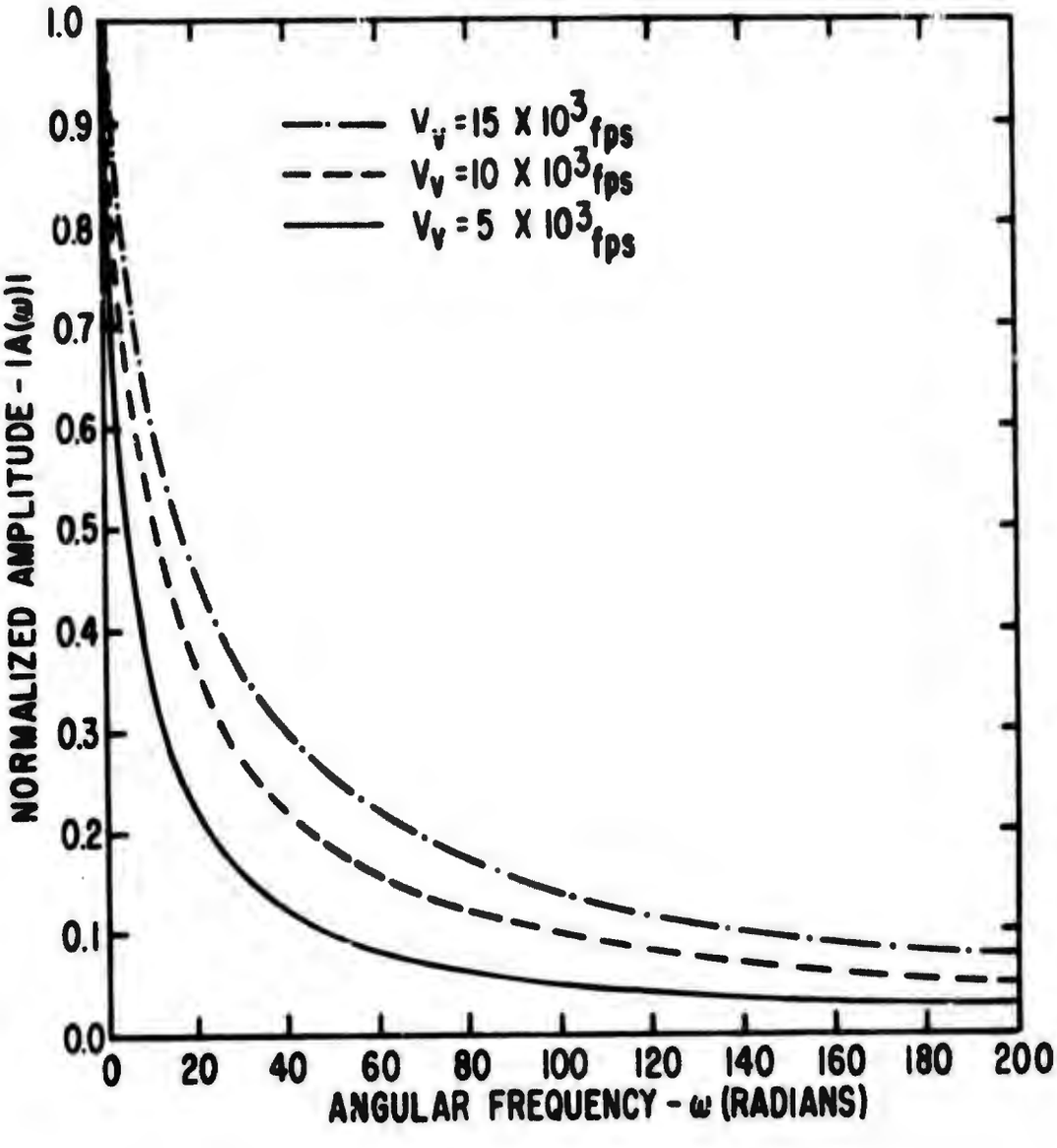

Figure 8. Amplitude Spectra for h_f = 1000 feet and Three Velocities

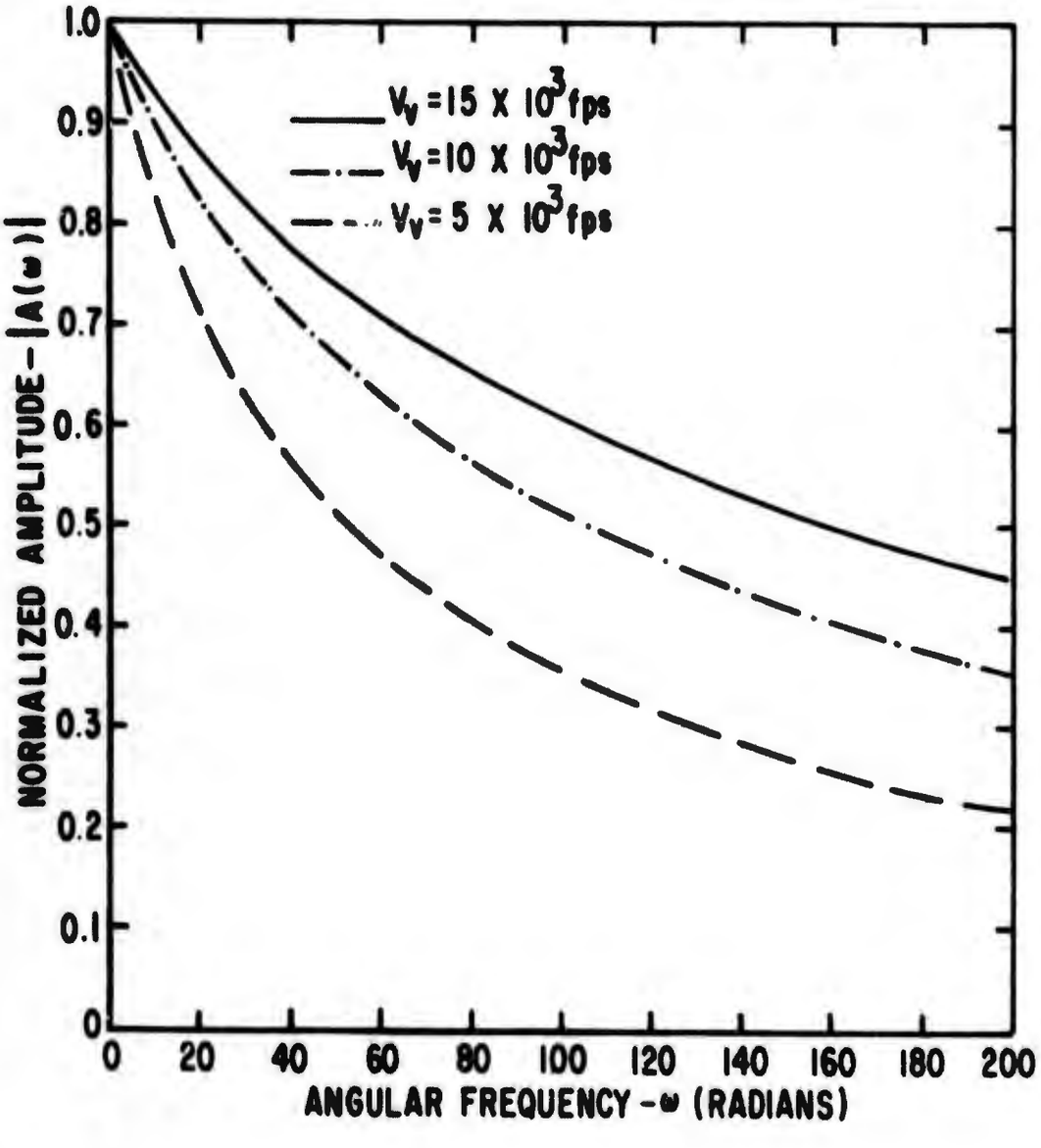

Figure 9. Amplitude Spectra for h_f = 100 feet and Three Velocities

The amplitude and phase spectra are determined from

$$A(\omega) = \int_{o}^{t_f} \frac{1}{\left(h_o - V_z t\right)^2} e^{-j\omega t} \, dt$$

where

$$t_f = \frac{h_o - h_f}{V_z}$$

3. A(t) Phase Spectrum

A single plot of phase versus frequency was obtained. This plot is shown in figure 10 for $h_o = 10^5$ feet, $h_f = 10^2$ feet, and a velocity of 5×10^3 fps. The spectrum is a linear function of frequency as in Appendix I.

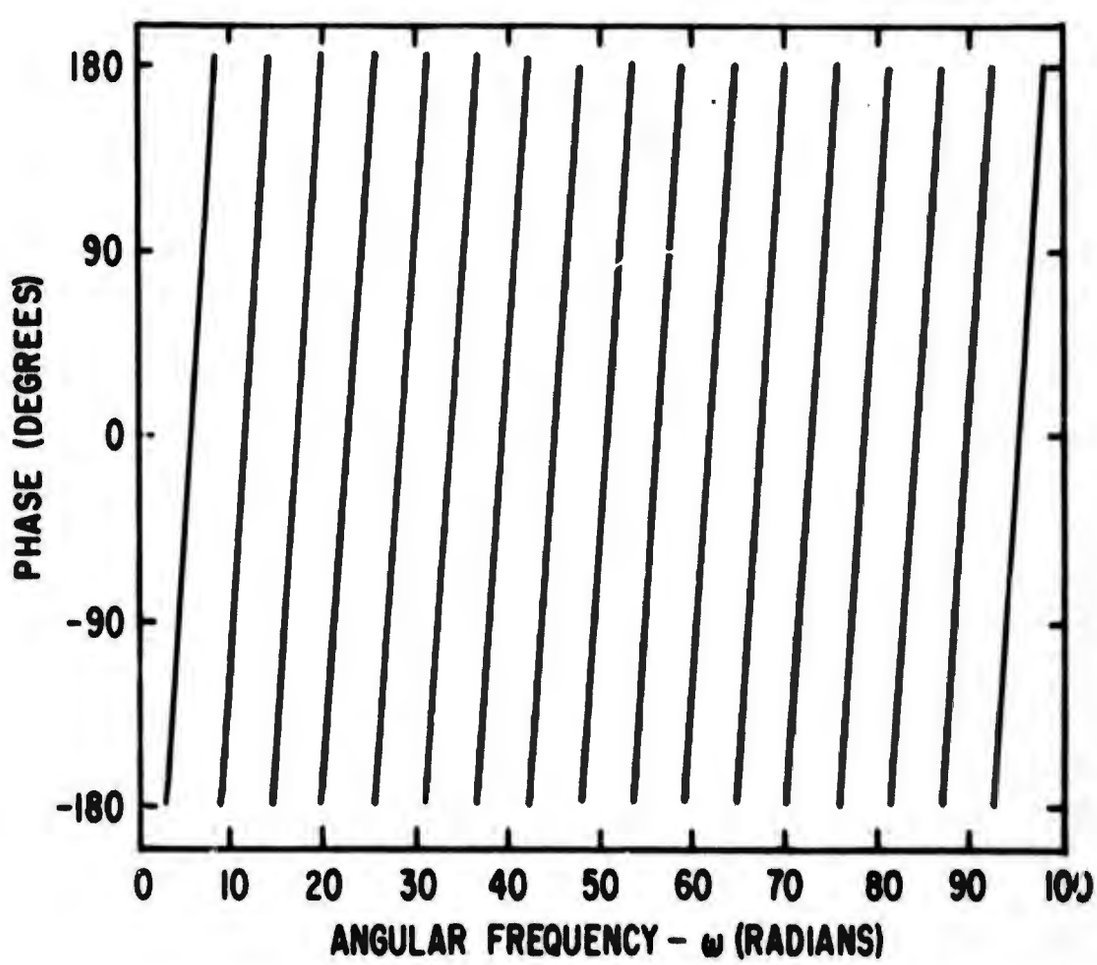

Figure 10. Phase Spectrum for $h_f = 100$ feet and $V_v = 5 \times 10^3$ fps

4. Velocity Spread

The range of velocity components to each point on the surface is derived from

$$V_c = |V|(\sin \gamma \sin \delta + \cos \gamma \cos \delta \sin \theta)$$

(see Appendix II). Figures 11 through 19 show the velocity components on the surface for flight path angles, γ, from 30° to 90° and vertical velocities of 5×10^3 fps, 10×10^3 fps, and 15×10^3 fps, as a function of δ. The flight path velocities, V_{fp}, are noted in the figure. These latter velocities are obtained for $\theta = -90°$ and $+90°$ only. For $\gamma = 90°$, we can see that the velocity components are symmetrically distributed about the origin noted in equation (6).

5. Comparison of Doppler and Amplitude Modulation Spectrum Spreading

To determine the degree of spectrum spreading that might be expected from both increasing amplitude and the Doppler effect, particular system parameters were selected. The results are tabulated in table I.

From table I we can conclude that greater spreading will occur for wide beamwidths and low final altitudes and that the spreading decreases for narrow beamwidths and higher final altitudes.

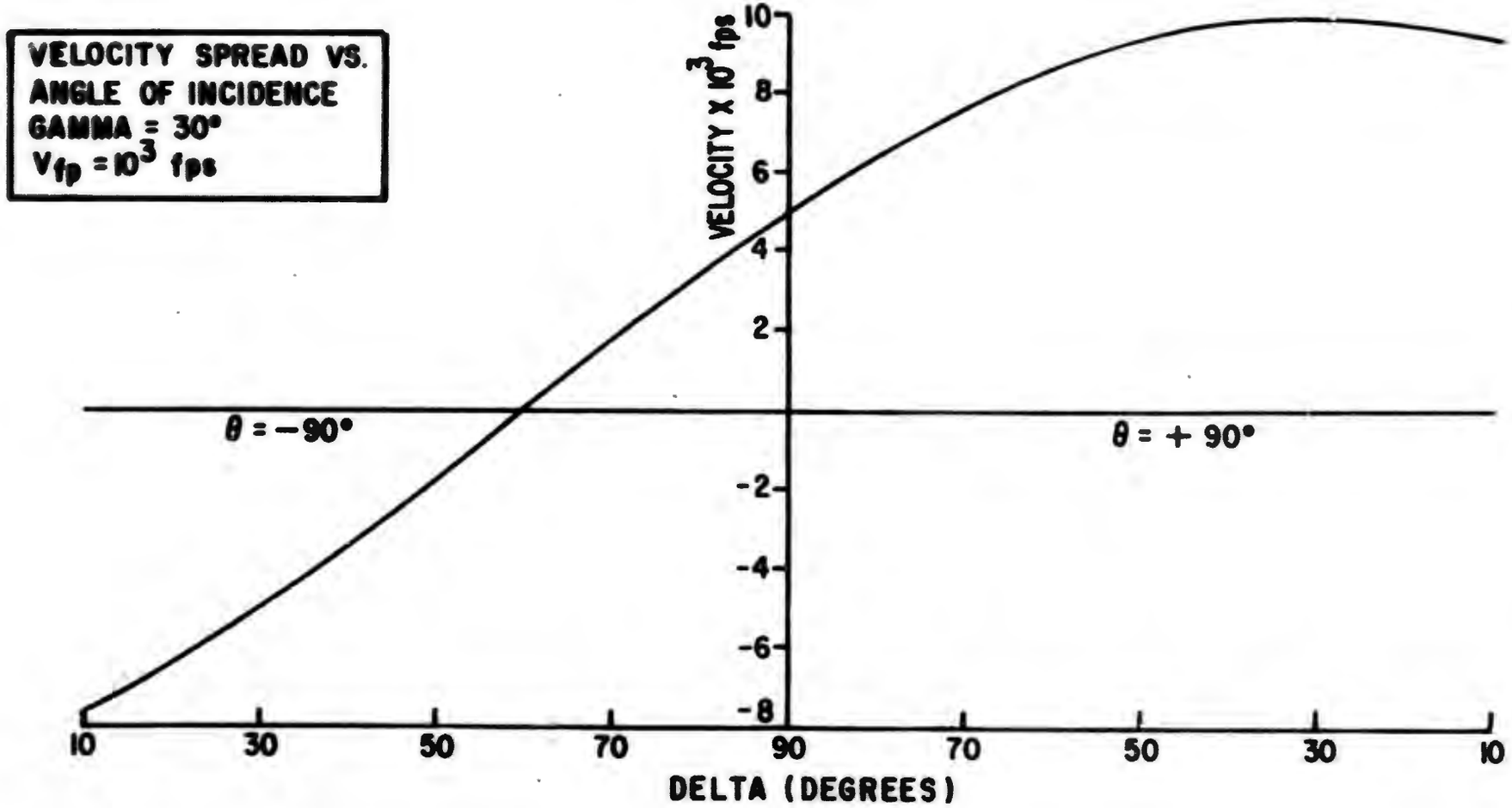

Figure 11. Velocity Spread for $\gamma = 30°$ and $V_v = 5 \times 10^3$ fps

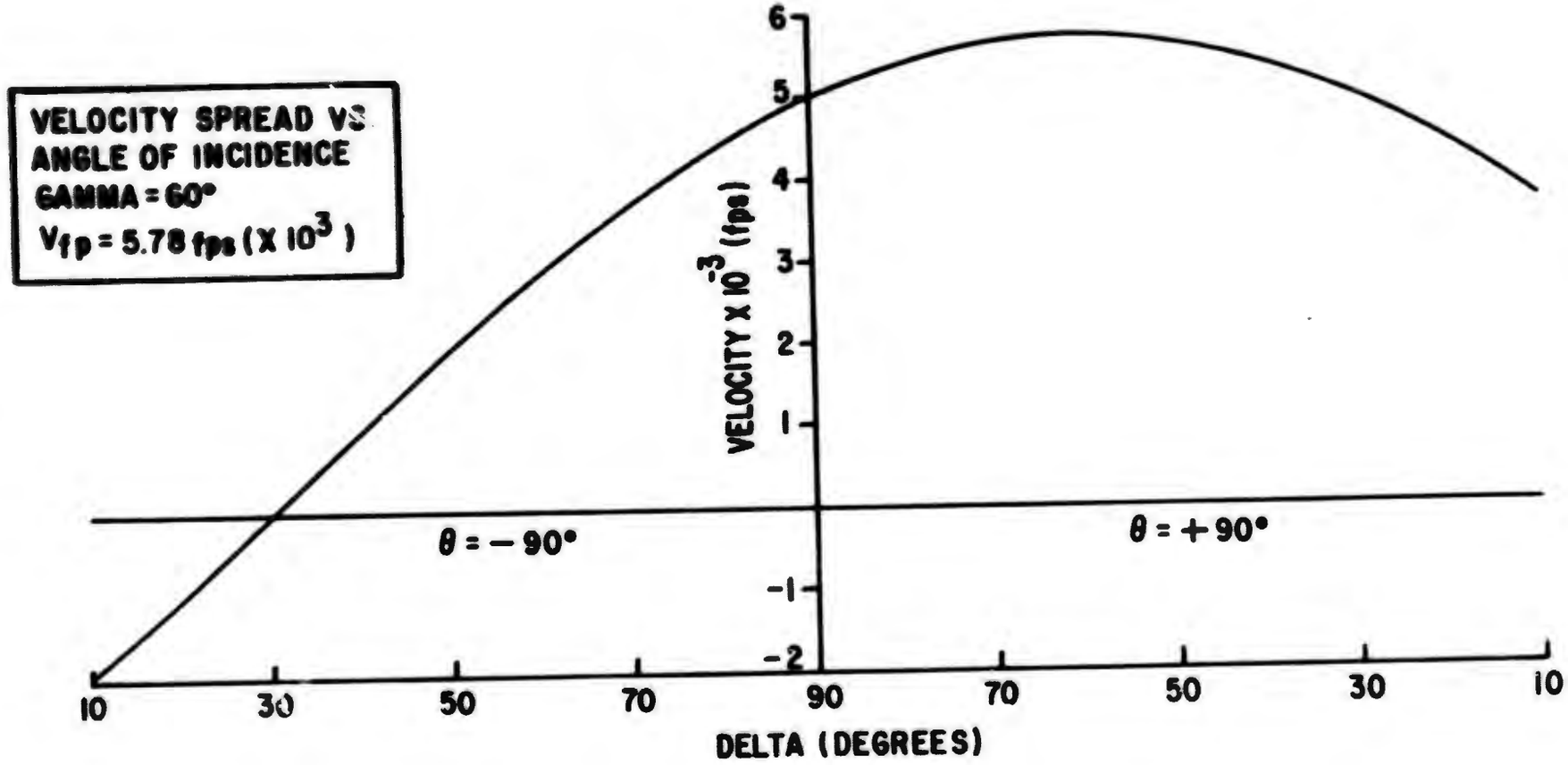

Figure 12. Velocity Spread for $\gamma = 60°$ and $V_v = 5 \times 10^3$ fps

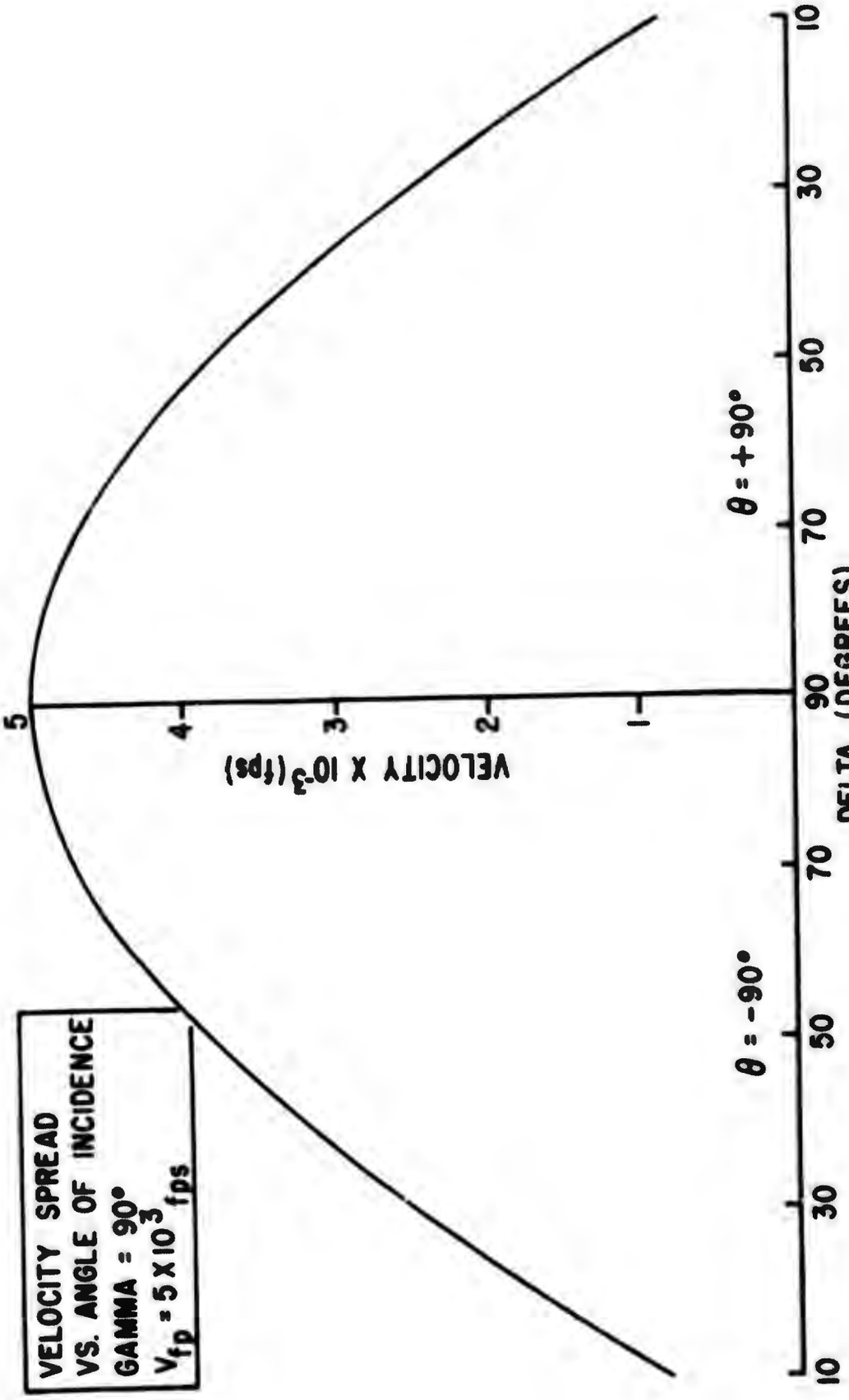

Figure 13. Velocity Spread for $\gamma = 90°$ and $V_v = 5 \times 10^3$ fps

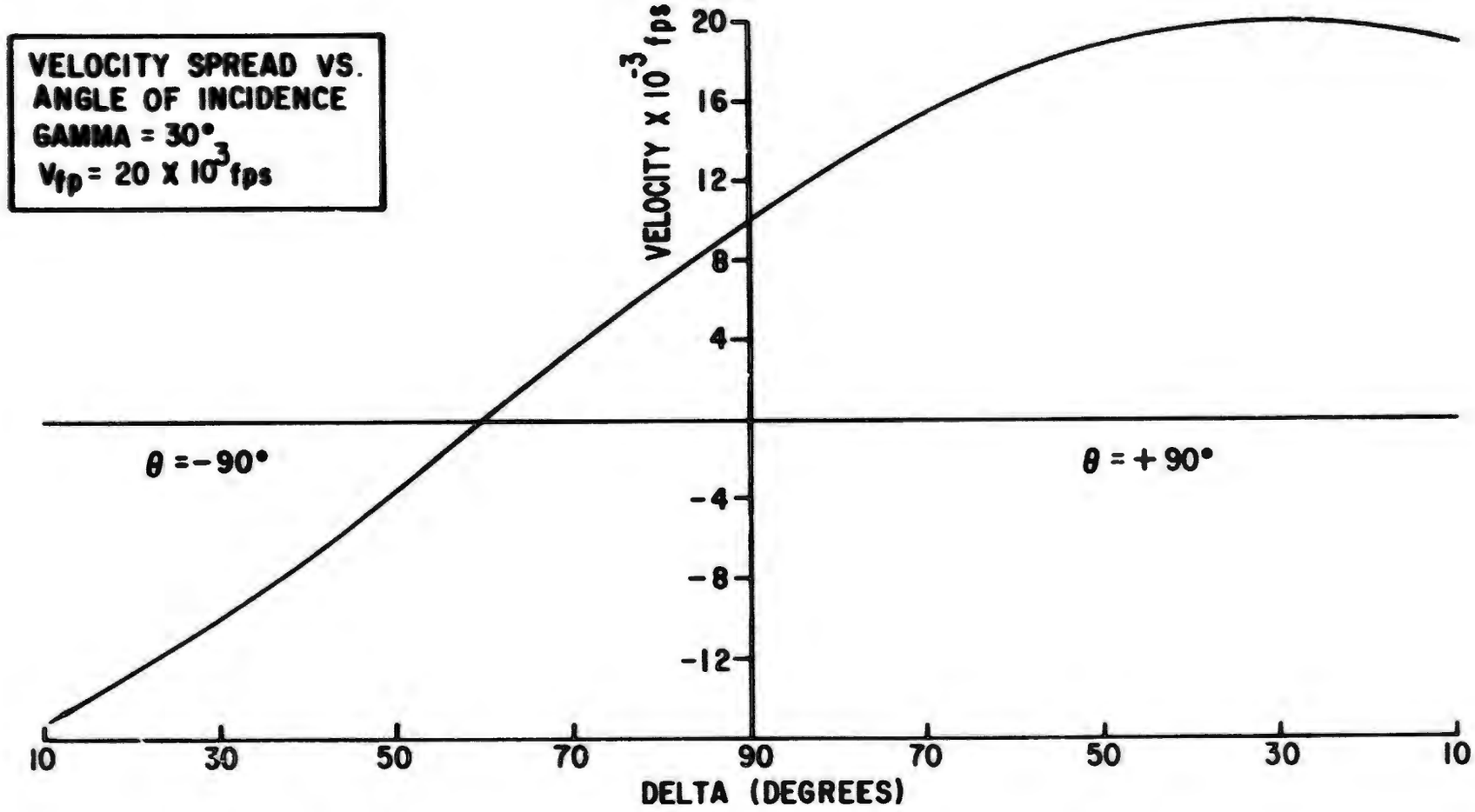

Figure 14. Velocity Spread for $\gamma = 30°$ and $V_v = 10 \times 10^3$ fps

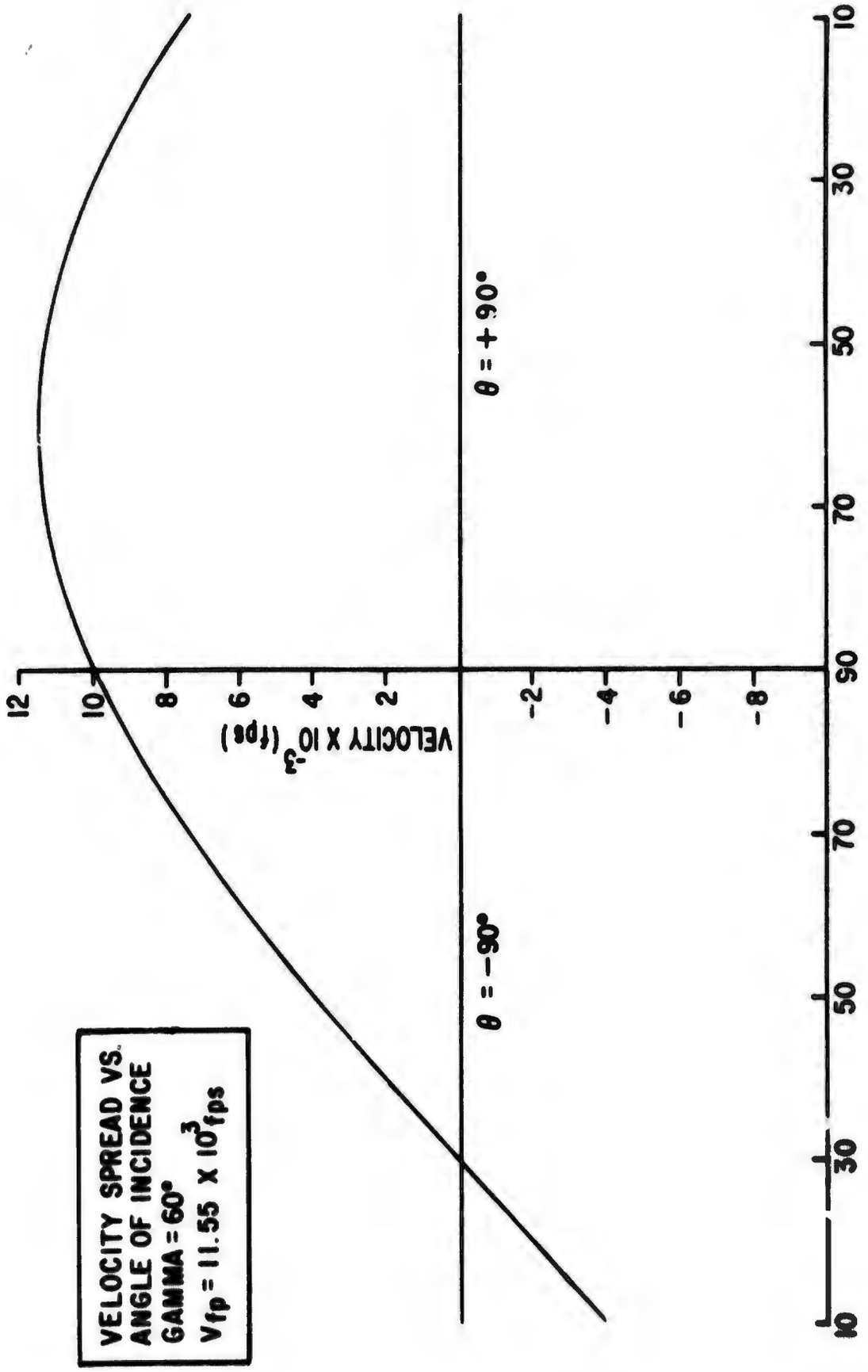

Figure 15. Velocity Spread for γ = 60° and V_v = 10 x 10^3 fps

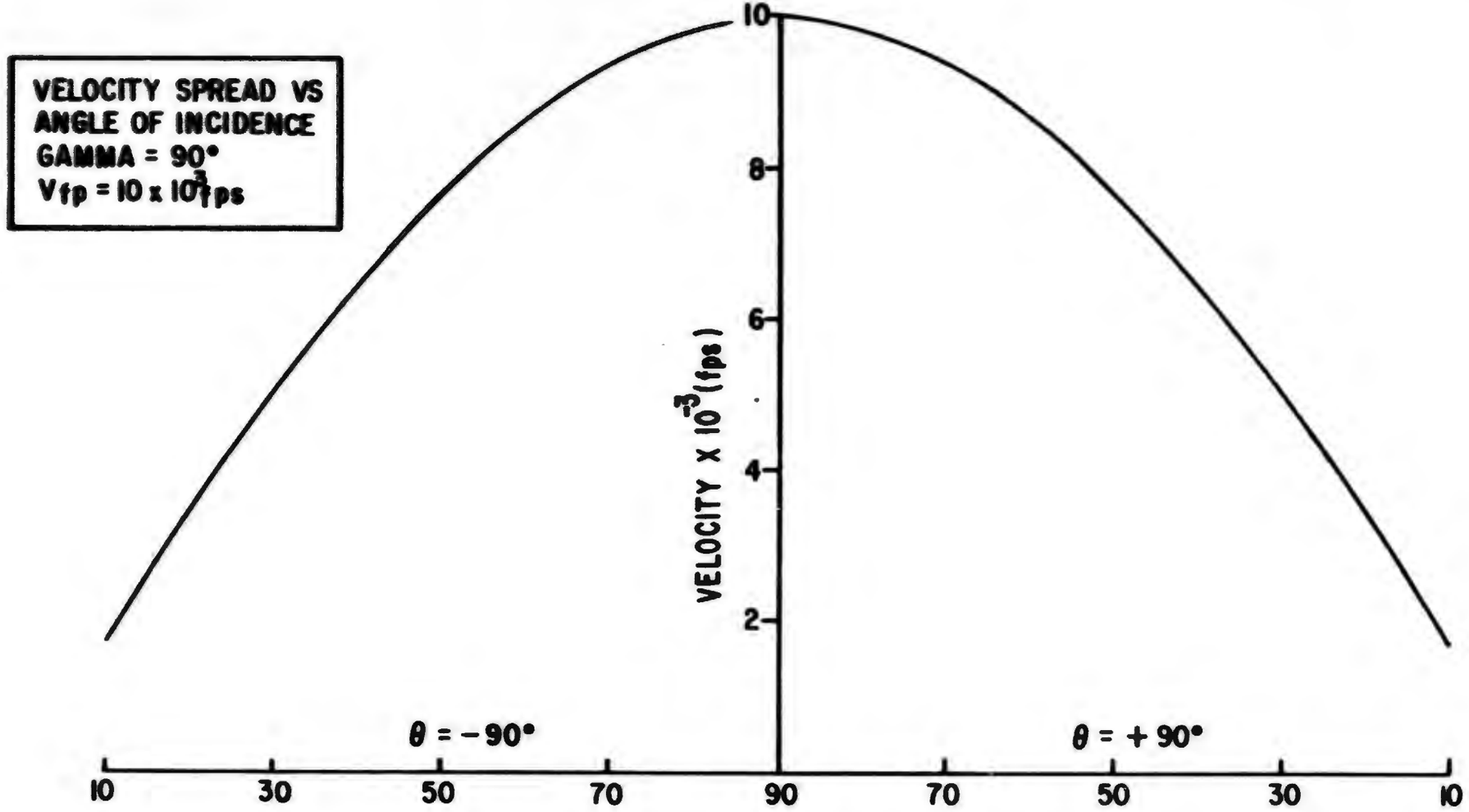

Figure 16. Velocity Spread for $\gamma = 90°$ and $V_v = 10 \times 10^3$ fps

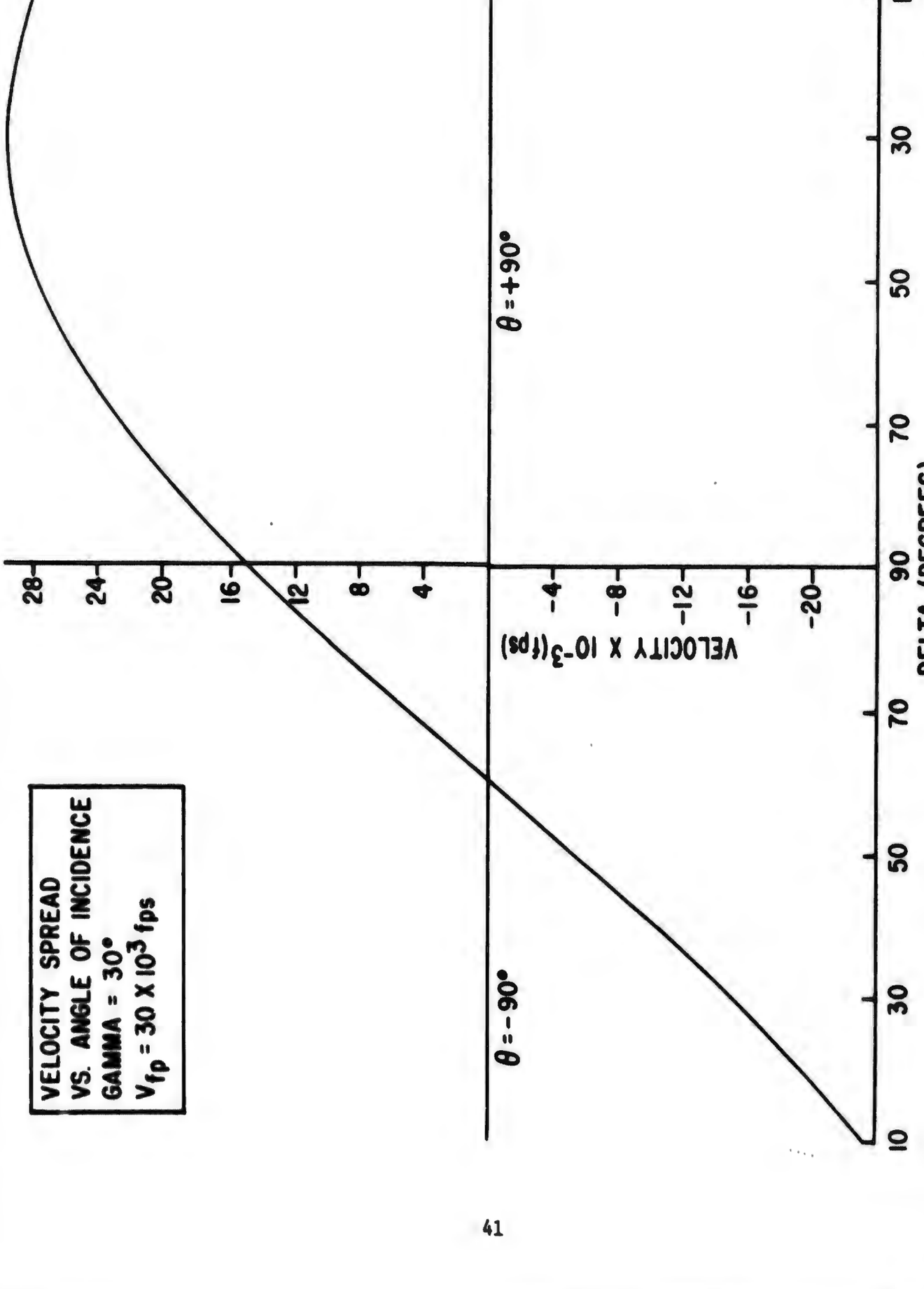

Figure 17. Velocity Spread for γ = 30° and V_v = 15 x 10^3 fps

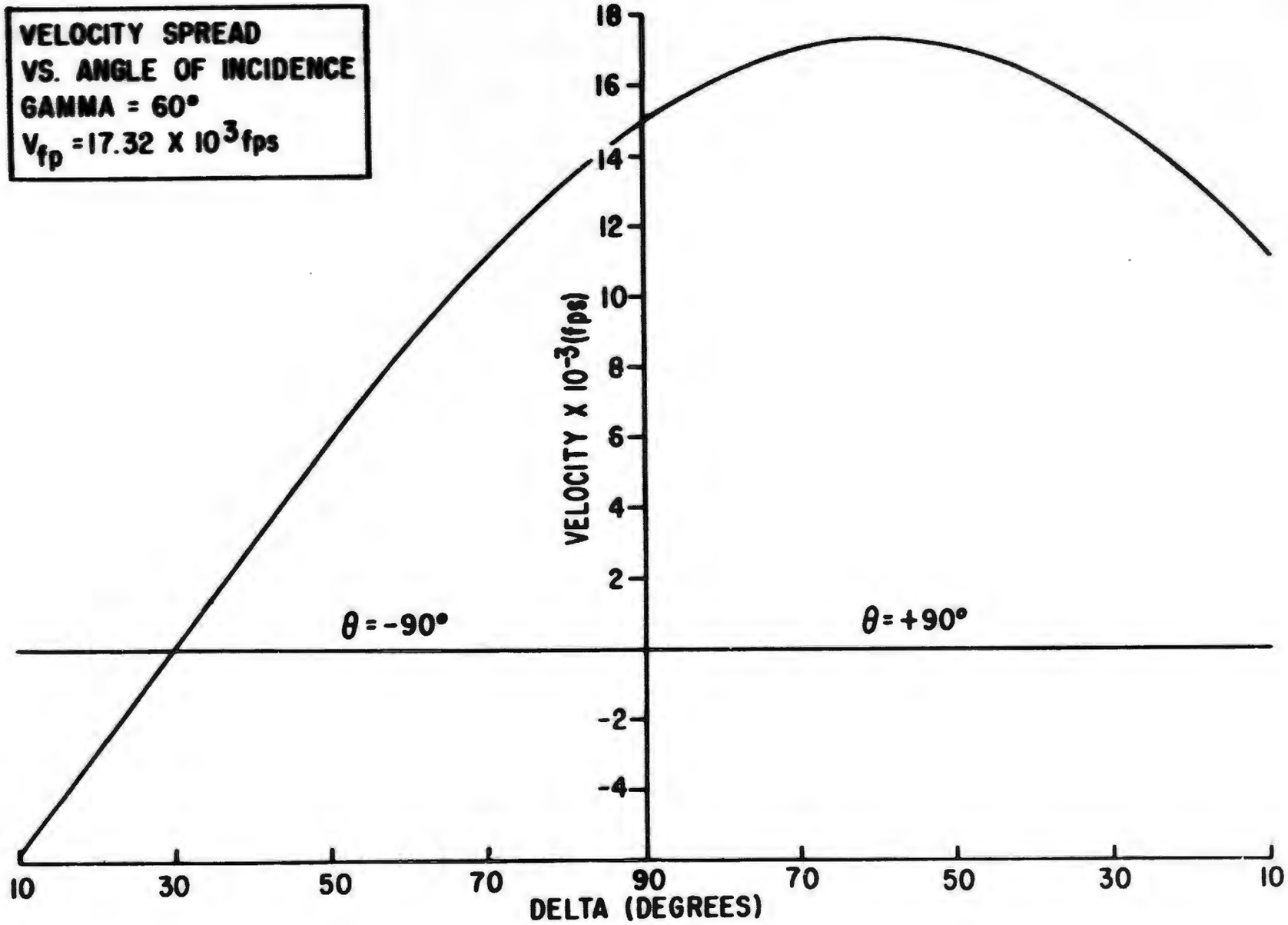

Figure 18. Velocity Spread for $\gamma = 60°$ and $V_v = 15 \times 10^3$ fps

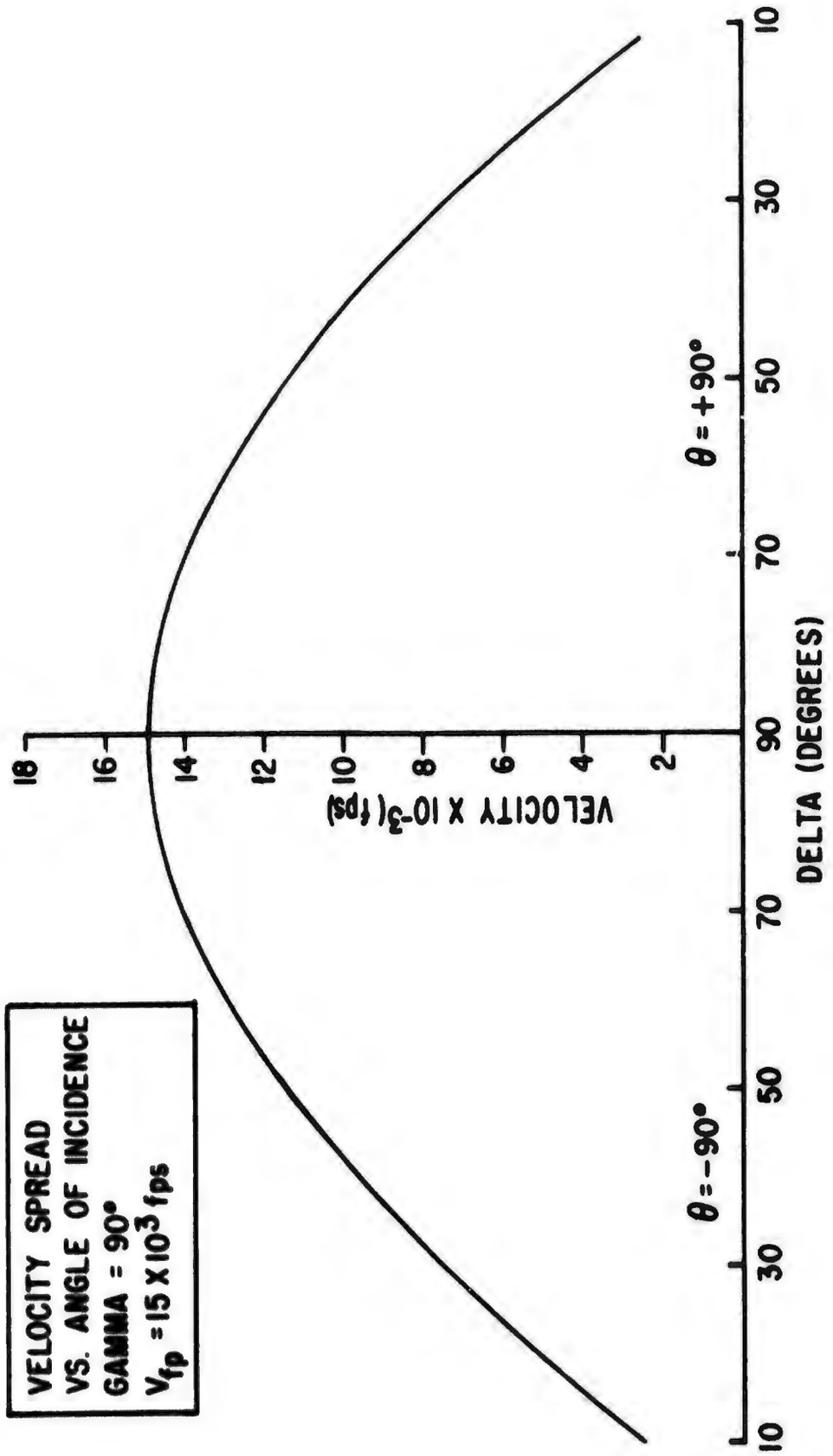

Figure 19. Velocity Spread for $\gamma = 90°$ and $V_v = 15 \times 10^3$ fps

Table I

FREQUENCY SPREADING CAUSED BY DOPPLER EFFECT AND INCREASING AMPLITUDE

	Total Doppler at $\gamma = 90°$		Increasing amplitude at 50% width	
Velocity (fps)	β (degrees)	$f_d \times 10^3$ Hz	h_f (feet)	$f_a \times 10^3$ Hz
			10	0.2
5×10^3	5	0.06	25	0.07
	60	5.00	100	0.017
			10	0.4
10×10^3	5	0.1	25	0.13
	60	10.0	100	0.037
			10	0.5
15×10^3	5	0.2	25	0.20
	60	15.0	100	0.052

SECTION VII

DETERMINING THE EFFECT OF THE REFLECTED SIGNAL ON A RECEIVING SYSTEM

In the previous sections, we have obtained equations to define the received signal as it is reflected from a smooth plane. In section II the transmission geometry was defined and an expression (equation (7)) defining the received signal was derived. In section III the return signal was defined in terms of the amplitude and delay to and from the reflecting surface. The amplitude was obtained from the radar equation. Thus, equations defining the received signal as a function of time were obtained (equations (35), (37), and (38)). In sections IV and V the signal returned from a point target and a thin reflecting strip was analyzed and the results were used in section VI in obtaining concrete results for the amount of distortion that may be expected because of rate of change of range and because of the Doppler effect.

In this section we shall utilize the results from the previous sections to show (at least qualitatively) the effect of the distorted return signal on a postulated receiving system. As mentioned previously, the receiver postulated here is selected only for the purpose of showing the consequences of receiving and processing a signal as hypothesized in this paper. A system description will first be presented and then the system analysis will be carried out. Figure 20 is a diagram of the system to be analyzed.

1. System Description

a. Transmitter

We shall assume that the transmitter includes a modulating signal, a carrier signal, a modulator, and all required amplifiers. In particular, we shall assume that the transmitted signal can be represented as

$$S_t(t) = A_o \cos\left[\omega_o t + \psi(t)\right] \tag{65}$$

where

$$\psi(t) = m_f \int_o^t g(\tau)\, d\tau$$

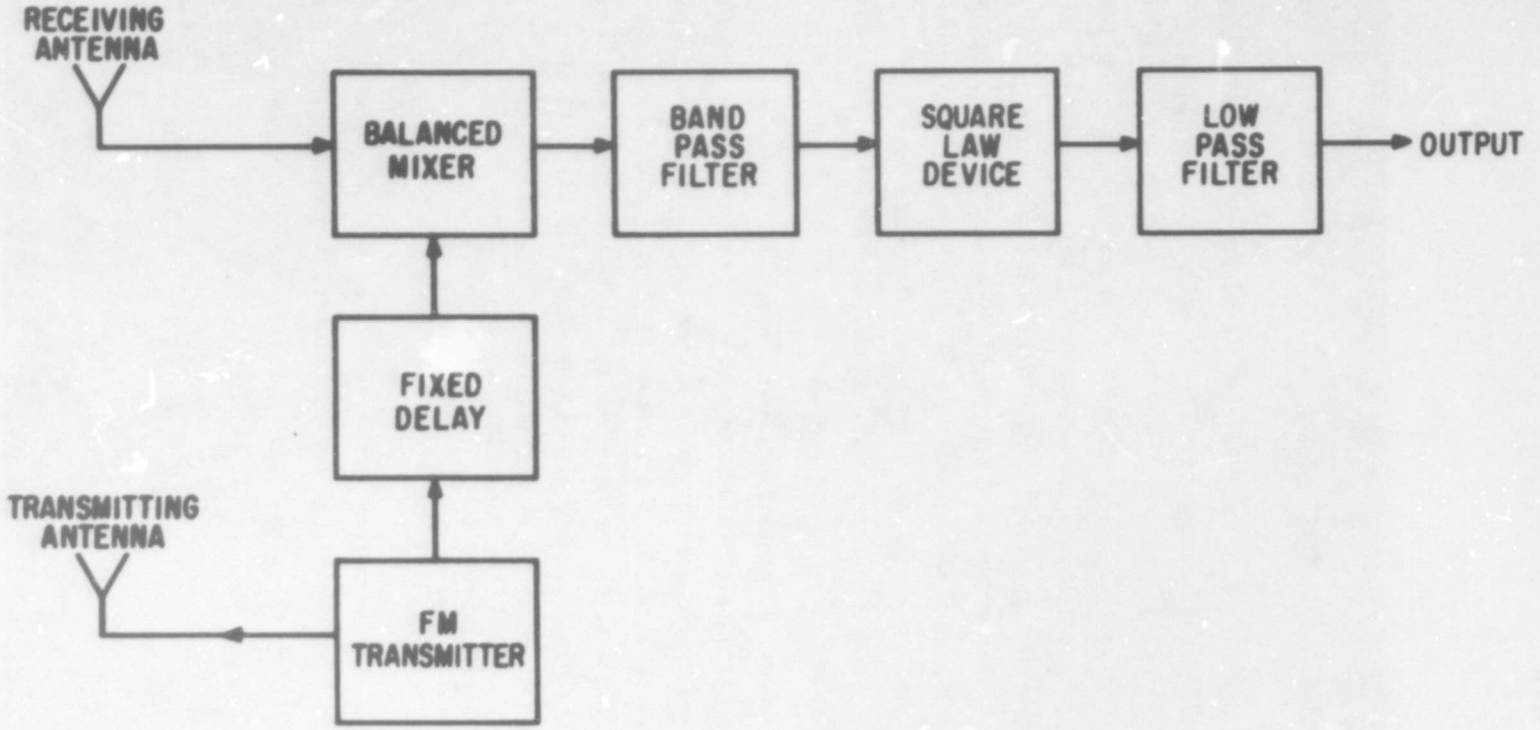

Figure 20. FM System Used for Signal Analysis

For simplicity we let

$$g(t) = \cos \omega_m t$$

and equation (1) is written as

$$S_t(t) = A_o \cos \left[\omega_o t + B \sin \omega_m t\right] \tag{66}$$

where $B = m_f/\omega_m$ (peak frequency deviation) with $\omega_o >> \omega_m$.

b. Fixed Delay

A sample of the instantaneous transmitted signal is taken and is delayed by a fixed amount τ_o. This fixed delay is useful in maximizing the system output at a fixed altitude. A variable delay could just as well be used, but the analysis is simpler if a fixed delay is used.

c. Balanced Mixer

The received signal, which is a delayed and attenuated version of the transmitted signal, is multiplied with the delayed sample of the transmitted signal in the balanced mixer. The output of the balanced mixer contains the sum and differences of all frequency components being multiplied. The balanced mixer translates high carrier frequencies to lower frequencies.

d. Bandpass Filter

The bandpass filter selects the lower difference frequencies provided by the balanced mixer.

e. Square-Law Device

The function of the square-law device is to separate range information from the difference frequency carrier as provided by the bandpass filter. The range information at this stage is contained in the amplitude of the signal caused by the varying range delay and range attenuation.

f. Low-Pass Filter

The low-pass filter selects the low-frequency range information as separated by the square-law device and provides a signal to decision circuits which follow. The decision functions will not be discussed.

2. The Method of Analysis

We shall first analyze the system by assuming that the signal is reflected from a single point on the surface. Next, we shall discuss the effect of signals from two or more points. We shall base the analysis on the Fourier transform method, obtaining amplitude and phase spectra for each function block. The characteristics of the filters will be assumed to be ideal, and will be described when appropriate.

If the transmitted signal is

$$S_t(t) = A_o \cos \left(\omega_o t + B \sin \omega_m t\right)$$

then the received signal from a point target is

$$S_r(t) = A(t) \cos \left\{\omega_o \left[t - \tau(t)\right] + B \sin \omega_m \left[t - \tau(t)\right]\right\} \qquad (67)$$

The sampled signal after a fixed delay of τ_o is

$$S_d(t) = \cos \left[\omega_o \left(t - \tau_o\right) + B \sin \omega_m \left(t - \tau_o\right)\right] \qquad (68)$$

The sampled signal amplitude (equation (68)) has been normalized to unity. Equation (67) may be expanded as

$$S_r(t) = A(t) \left\{\cos \omega_o \left[t - \tau(t)\right] \cos \left[B \sin \omega_m \left[t - \tau(t)\right]\right]\right.$$

$$\left. - \sin \omega_o \left[t - \tau(t)\right] \sin \left[B \sin \omega_m \left[t - \tau(t)\right]\right]\right\} \qquad (69)$$

By using the well known relations

$$\cos (x \sin \theta) = J_o (x) + 2 \sum_{n=1}^{\infty} J_{2n} (x) \cos 2n\theta$$

and

$$\sin (x \sin \theta) = 2 \sum_{n=0}^{\infty} J_{2n+1} (x) \sin (2n + 1) \theta$$

where $J_n(x)$ is the Bessel function of the first kind and order n, we can write equation (69) as

$$S_r(t) = A(t) \left\{ \cos \omega_o [t - \tau(t)] \left[J_o(B) + 2 \sum_{n=1}^{\infty} J_{2n}(B) \cos 2n \left[\omega_m [t - \tau(t)] \right] \right] - \sin \omega_o [t - \tau(t)] \cdot \left[2 \sum_{n=0}^{\infty} J_{2n+1}(B) \sin (2n + 1) \omega_m [t - \tau(t)] \right] \right\}$$

By substituting

$$\tau(t) = t_o - \lambda t, \text{ where } \lambda = \frac{2V}{c}$$

we obtain

$$S_r(t) = A(t) J_o(B) \cos \left[\left(\omega_o + \lambda \omega_o \right) t - \omega_o t_o \right] + 2A(t) \sum_{n=1}^{\infty} J_{2n}(B) \cos \left[\left(\omega_o + \lambda \omega_o \right) t - \omega_o t_o \right] \cos 2n \left[\left(\omega_m + \lambda \omega_m \right) t - \omega_m t_o \right] - 2A(t) \sum_{n=0}^{\infty} J_{2n+1}(b) \sin \left[\left(\omega_o + \lambda \omega_o \right) t - \omega_o t_o \right] \sin \left\{ (2n + 1) \left[\left(\omega_m + \lambda \omega_m \right) t - \omega_m t_o \right] \right\} \quad (70)$$

Similarly, equation (68) may be written as

$$S_d(t) = J_o(B) \cos\left(\omega_o t - \omega_o \tau_o\right) + 2 \sum_{n=1}^{\infty} J_{2n}(B) \cos\left(\omega_o t - \omega_o \tau_o\right) \cos 2n\left(\omega_m t - \omega_m \tau_o\right) - 2 \sum_{n=0}^{\infty} J_{2n+1}(B) \sin\left(\omega_o t - \omega_o \tau_o\right) \sin (2n+1)\left(\omega_m t - \omega_m \tau_o\right) \tag{71}$$

Equation (70) is composed of an infinite number of frequency components, each of which is amplitude-modulated by A(t). Each component is in the form

$$e(t) = g(t) \cos\left(\omega_o t - \phi\right) \tag{72}$$

which is a double side band (DSB) modulated carrier. The Fourier transform of equation (72) is

$$E(\omega) = 1/2 \left\{ e^{-j\phi} G\left(\omega - \omega_o\right) + e^{+j\phi} G\left(\omega + \omega_o\right) \right\} \tag{73}$$

By using equation (73) and the convolution theorem, we may write equation (70) as

$$S_r(\omega) = \frac{J_o(B)}{2} \left\{ e^{-j\omega_o t_o} A\left(\omega - \omega_o - \omega_{od}\right) + e^{j\omega_o t_o} A\left(\omega + \omega_o + \omega_{od}\right) \right\} + \sum_{n=1}^{\infty} J_{2n}(B) \left\{ e^{-j\left(\omega_o t_o + 2n\omega_m t_o\right)} A\left(\omega - \omega_o - \omega_{od} - 2n\left(\omega_m + \omega_{md}\right)\right) \right.$$

$$+ e^{j\left(\omega_o t + 2n\omega_m t_o\right)} A\left(\omega + \omega_o + \omega_{od} + 2n\left(\omega_m + \omega_{md}\right)\right)\Big\}$$

$$+ \sum_{n=1}^{\infty} J_{2n}(B)\left\{e^{-j\left(\omega_o t_o - 2n\omega_m t_o\right)} A\left(\omega - \omega_o - \omega_{od} + 2n\left(\omega_m + \omega_{md}\right)\right)\right.$$

$$\left. + e^{j\left(\omega_o t_o - 2n\omega_m t_o\right)} A\left(\omega + \omega_o + \omega_{od} - 2n\left(\omega_m + \omega_{md}\right)\right)\right\}$$

$$+ \sum_{n=0}^{\infty} J_{2n+1}(B)\left\{e^{-j\left[\omega_o t_o + (2n+1)\omega_m t_o\right]} A\left(\omega - \omega_o - \omega_{od} - (2n+1)\left(\omega_m + \omega_{md}\right)\right)\right.$$

$$\left. + e^{j\left[\omega_o t_o + (2n+1)\omega_m t_o\right]} A\left(\omega + \omega_o + \omega_{od} + (2n+1)\left(\omega_m + \omega_{md}\right)\right)\right\}$$

$$- \sum_{n=0}^{\infty} J_{2n+1}(B)\left\{e^{-j\left[\omega_o t_o - (2n+1)\omega_m t_o\right]} A\left(\omega - \omega_o - \omega_{od} + (2n+1)\left(\omega_m + \omega_{md}\right)\right)\right.$$

$$\left. + e^{j\left[\omega_o t_o - (2n+1)\omega_m t_o\right]} A\left(\omega + \omega_o + \omega_{od} - (2n+1)\left(\omega_m + \omega_{md}\right)\right)\right\} \qquad (74)$$

where

$$\omega_{od} = \lambda\omega_o \text{ and } \omega_{md} = \lambda\omega_m \qquad (75)$$

The first term in equation (74) is the spectrum of the modulating range function A(t) shifted symmetrically about the origin by $\omega_o + \omega_{od}$, where ω_{od} is the Doppler shift, and the amplitude is given by $J_o(B)/2$. The second and third terms are summations of an infinite number of sum and difference frequencies of amplitude $J_{2n}(B)$ shifted symmetrically about the origin and centered at $\omega + \omega_{od}$; each frequency component is modulated by A(t). The fourth and fifth terms are identical to the second and third terms except they are comprised of

of the odd harmonics. The phase of each component is determined by the exponential factor.

The Fourier transform of equation (71) is

$$S_d(\omega) = \frac{J_o(B)}{2}\left\{e^{-j\omega_o\tau_o}\,\delta\left(\omega-\omega_o\right)+e^{j\omega_o\tau_o}\,\delta\left(\omega+\omega_o\right)\right\}$$

$$+\sum_{n=1}^{\infty}J_{2n}(B)\left\{e^{-j\left(\omega_o\tau_o+2n\omega_m\tau_o\right)}\,\delta\left(\omega-\omega_o-2n\omega_m\right)\right.$$

$$\left.+e^{j\left(\omega_o\tau_o+2n\omega_m\tau_o\right)}\,\delta\left(\omega+\omega_o+2n\omega_m\right)\right\}$$

$$+\sum_{n=1}^{\infty}J_{2n}(B)\left\{e^{-j\left(\omega_o\tau_o-2n\omega_m\tau_o\right)}\,\delta\left(\omega-\omega_o+2n\omega_m\right)\right.$$

$$\left.+e^{j\left(\omega_o\tau_o-2n\omega_m\tau_o\right)}\,\delta\left(\omega+\omega_o-2n\omega_m\right)\right\}$$

$$+\sum_{n=0}^{\infty}J_{2n+1}(B)\left\{e^{-j\left[\omega_o\tau_o+(2n+1)\omega_m\tau_o\right]}\,\delta\left(\omega-\omega_o-(2n+1)\,\omega_m\right)\right.$$

$$\left.+e^{j\left[\omega_o\tau_o+(2n+1)\omega_m\tau_o\right]}\,\delta\left(\omega+\omega_o+(2n+1)\,\omega_m\right)\right\}$$

$$-\sum_{n=0}^{\infty}J_{2n+1}(B)\left\{e^{-j\left[\omega_o\tau_o-(2n+1)\omega_m\tau_o\right]}\cdot\,\delta\left(\omega-\omega_o+(2n+1)\,\omega_m\right)\right.$$

$$+ e^{j\left[\omega_o \tau_o - (2n+1)\omega_m \tau_o\right]} \delta\left(\omega + \omega_o - (2n+1)\,\omega_m\right)\Bigg\} \qquad (76)$$

Equation (76) differs from equation (74) in that the terms in equation (76) have not been shifted by the Doppler effect and the individual frequency components are not modulated.

Thus, from equation (74), we can see that the effect of transmitting an FM signal to a point target from a moving vehicle is to spread the individual frequency components over a wider frequency range than if the relative velocity were zero.

The amplitude spectra of the range function A(t) and the received signal are shown in figures 21 and 22 (compare with figures 8 and 9). The greater the relative velocity the wider the range function spectrum will become. At very high velocities (see section VI) the line spectra of the received signal overlap and cause added distortion.

3. Determination of A(t) Spectrum

We have found that the received amplitude is a function of angle of incidence and time and is represented by

$$A(t) = \frac{K(\delta)}{\left(h_o - V_z t\right)^2} \qquad (77)$$

The Fourier transform of A(t) is given by

$$A(\omega) = \int_{-\infty}^{+\infty} A(t)\, e^{-j\omega t}\, dt \qquad (78)$$

For our problem, we shall consider the following limits on A(t):

$$A(t) = \frac{K(\delta)}{\left(h_o - V_z t\right)^2} \quad \text{for } 0 \leq t \leq t_f$$

$$A(t) = 0 \quad \text{otherwise} \qquad (79)$$

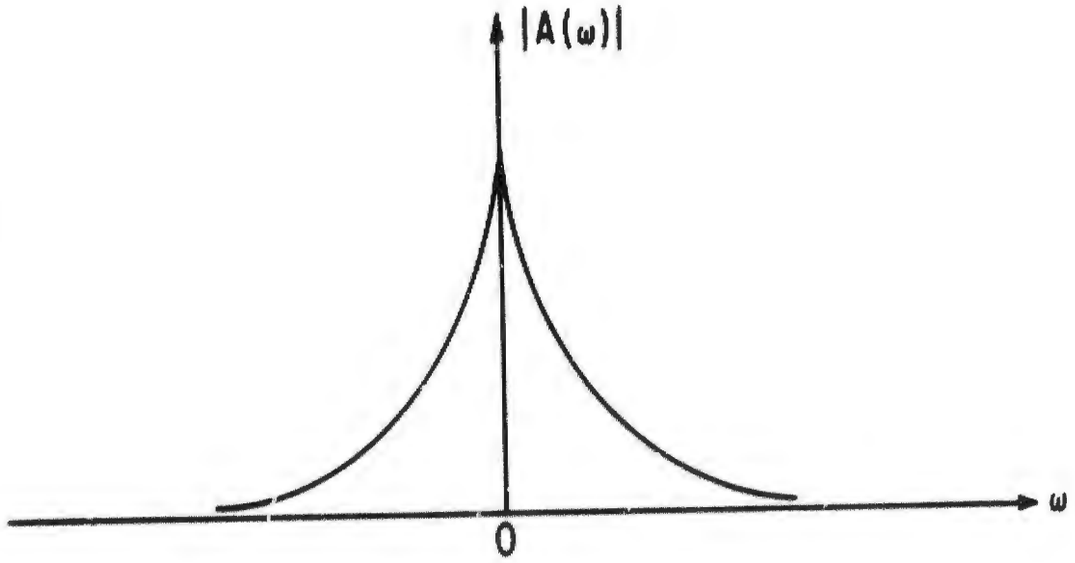

Figure 21. Amplitude Spectrum of the Range Function A(t)

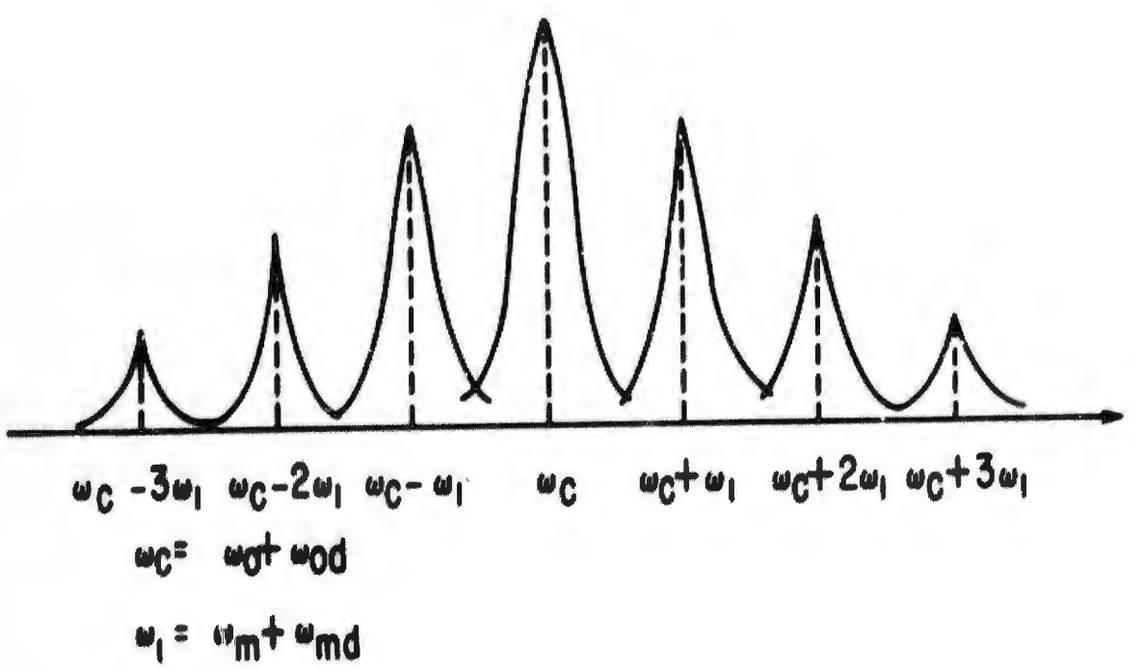

Figure 22. Amplitude Spectrum of the Received FM Signal Showing Only a Few Spectral Lines

where

$$t_f < \frac{h_o}{V_z} \tag{80}$$

The quantity t_f, as we discussed previously, must not only meet the condition specified by equation (80), but it must also limit consideration of equation (79) to points outside the electromagnetic near field since equation (79) is not defined in that region. Therefore, by substituting equation (79) into equation (78), we obtain

$$A(\omega) = \int_0^{t_f} \frac{K(\delta)}{\left(h_o - V_z t\right)^2} e^{-j\omega t}\, dt \tag{81}$$

The solution of equation (81) is an infinite series, but concrete results were obtained through computer methods. The numerical results were given in the previous section, and the general amplitude spectrum is given in figure 21 for comparison. In figure 22 we have shown a part of the amplitude spectrum of the received FM signal with the spreading due to A(t) emphasized.

4. Analysis of the Receiver

a. Balanced Mixer Output

We have seen that the function of the balanced mixer (BM) was to multiply the received signal with the delayed signal, thus providing sum and difference frequencies of these two "mixed" signals at the BM output.

The BM output may be obtained by multiplying equation (70) and equation (71). The multiplication is carried out by first expanding each term in equation (70) and equation (71), then multiplying equation (70) and equation (71) term by term. The expansion and the multiplication are shown in Appendix III. Appendix III also shows the difference frequency part of the BM output.

We have considered the BM to be a linear multiplying element; therefore, the returned signals from many points may be treated separately and then summed. The only limitations imposed on the mixer by the received signal spreading is the maximum bandwidth, but because the mixer is usually a wideband device, the spreading will have a negligible affect on the mixer.

b. Bandpass Filter

We shall assume that the bandpass filter (BPF) tranfer function is composed of $H_1(\omega)$ and $H_2(\omega)$, as given in figures 23 and 24. Papoulis (Ref. 9) has shown that for an amplitude modulated input

$$f(t) = f_\ell(t) \cos \omega_o t \tag{82}$$

of carrier frequency equal to the center frequency ω_o of the filter, if

$$F_\ell(\omega) = 0 \text{ for } |\omega| > \omega_o - \omega_c \tag{83}$$

where ω_c is the filter cutoff frequency, then the BPF output is given by

$$g(t) = g_\ell(t) \cos \omega_o t \tag{84}$$

where

$$G_\ell(\omega) = H_\ell(\omega) F_\ell(\omega) \tag{85}$$

and $H_\ell(\omega)$ is the equivalent LPF transfer function. The equivalent LPF transfer function is shown in figure 25.

For our problem

$$f_B(t) = \frac{\left[J_o(B)\right]^2}{2} A(t) \cos \left[\lambda \omega_o t - \omega_o \left(t_o - \tau_o\right)\right] \tag{86}$$

is the input to the BPF (see Appendix III). We shall assume that all other BM output frequency components are attenuated completely. By using equations (82) and (84), the BPF output is then found to be

$$g_B(t) = \frac{\left[J_o(B)\right]^2}{2} A_B(t) \cos \left[\lambda \omega_o t - \omega_o \left(t_o - \tau_o\right)\right] \tag{87}$$

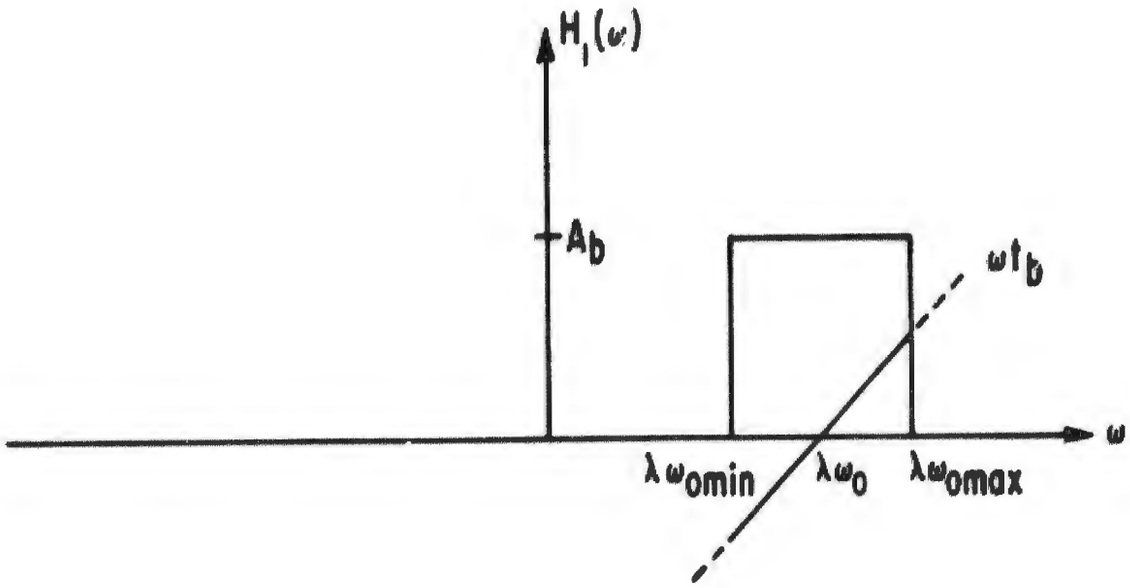

Figure 23. $H_1(\omega)$ Bandpass Filter Characteristic

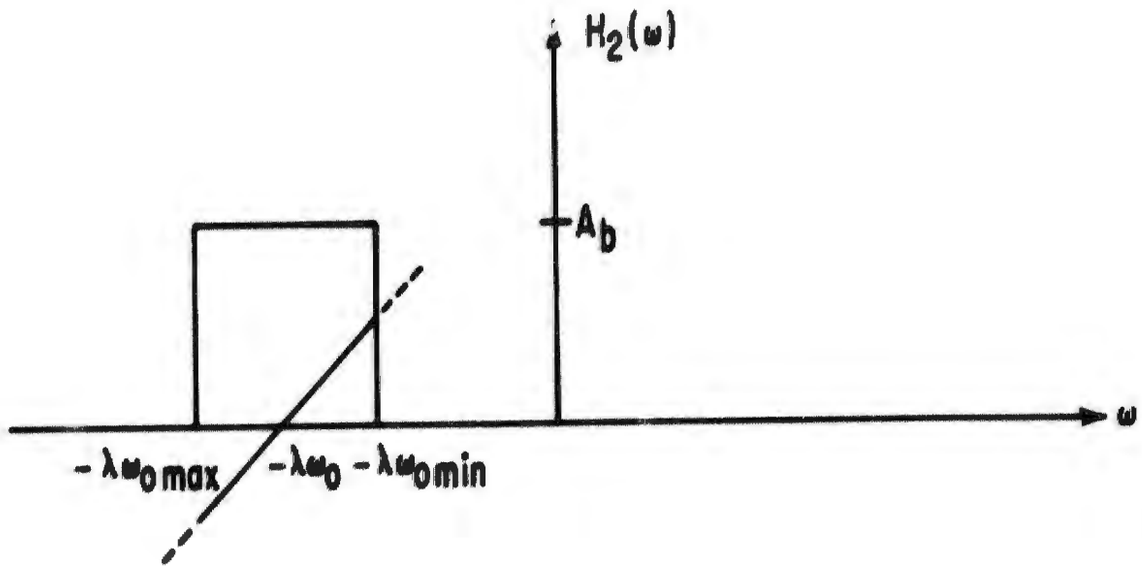

Figure 24. $H_2(\omega)$ Bandpass Filter Characteristic

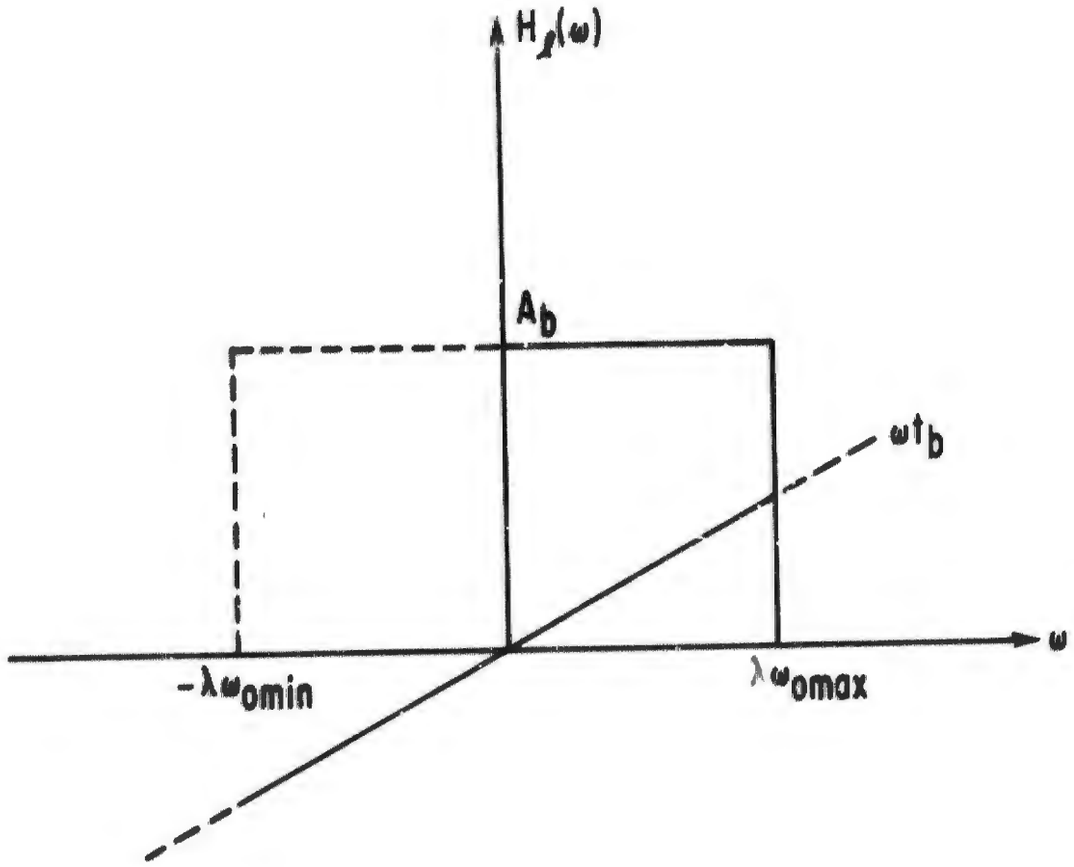

Figure 25. Equivalent Low-Pass Filter Characteristic

where

$$A_B(\omega) = H_\ell(\omega)\ A(\omega) \tag{88}$$

or from figure 25

$$H_\ell(\omega) = \begin{cases} A_o\ e^{-j\omega t_b} & \text{for } |\omega| < \lambda\omega_{o\,max} \\ 0 & \text{for } |\omega| > \lambda\omega_{o\,max} \end{cases} \tag{89}$$

equation (88) becomes

$$A_B(\omega) = A_o\ A(\omega)\ e^{-j\omega t_b} \tag{90}$$

Hence, if we use the shifting theorem, equation (90) may be written as

$$A_B(t) = A_o\, A\left(t - t_b\right) \tag{91}$$

Therefore, equation (87) becomes

$$g_B(t) = \frac{A_o\left[J_o(B)\right]^2}{2} A\left(t - t_b\right) \cos\left[\lambda\omega_o t - \omega_o\left(t_o - \tau_o\right)\right] \tag{92}$$

i.e., the output of the BPF is a delayed and attenuated version of the input.

From equation (92) we can see that the BPF output signal is in the form of a DSB modulated signal with the Doppler as the carrier and the range function $A\left(t - t_b\right)$ the modulating signal. Therefore, the BPF must be selected such that for a point target it will pass the $A\left(t - t_b\right)$ spectrum. For a return from many points on the reflecting surface, the bandwidth selection of the BPF becomes more severe. The first criterion in selecting the bandwidth is that the total Doppler spreading must be considered, and, second, the $A\left(t - t_b\right)$ band must be considered, i.e., the $A\left(t - t_b\right)$ due to each point on the reflecting surface are shifted by different amounts by the Doppler effect at that point.

c. Square-Law Device

Up to this point we have only considered linear operations on the received signal, making it possible to analyze the effect of the received signal from each point in the illuminated area and then summing the total signal to determine the total effect. Because the square-law device is non-linear, superposition does not hold, and the total signal must be considered in one operation. First, we shall consider the return from one point, then from many points.

From equation (92), the output from the BPF due to the return from a single point may be written as

$$g_{B1}(t) = \frac{A_o\left[J_o(B)\right]^2}{2} A_1\left(t - t_b\right) \cos\left[\lambda_1\omega_o t - \omega_o\left(t_{o1} - \tau_o\right)\right] \tag{93}$$

The output of the square-law device is obtained by squaring equation (93), i.e.,

$$g_{s1}(t) = \left[g_{B1}(t)\right]^2$$

$$= \frac{A_o^2\left[J_o(B)\right]^4}{4}\left[A_1\left(t - t_b\right)\right]^2 \cos^2\left[\lambda_1\omega_o t - \omega_o\left(t_{o1} - \tau_o\right)\right]$$

$$= \frac{A_o^2\left[J_o(B)\right]^4}{8}\left[A_1\left(t - t_b\right)\right]^2 \left\{1 + \cos 2\left[\lambda_1\omega_o t - \omega_o\left(t_{o1} - \tau_o\right)\right]\right\} \quad (94)$$

From equation (94) we see that the output from the square-law device caused by the return from a single point is composed of a low-frequency term and a high-frequency term. The low-frequency term is the A(t) spectrum while the high-frequency term is the A(t) spectrum shifted to the Doppler frequency $2\lambda_1\omega_o$.

The input to the square-law device caused by signals from two points on the surface is

$$g_{B1,2}(t) = \frac{A_o\left[J_o(B)\right]^2}{2}\left\{A_1\left(t - t_b\right)\cos\left[\lambda_1\omega_o t - \omega_o\left(t_{o1} - \tau_o\right)\right]\right.$$

$$\left. + A_2\left(t - t_b\right)\cos\left[\lambda_2\omega_o t - \omega_o\left(t_{o2} - \tau_o\right)\right]\right\} \quad (95)$$

The square-law output now becomes

$$g_{s1,2}(t) = \frac{A_o^2\left[J_o(B)\right]^4}{4}\left\{A_1\left(t - t_b\right)\cos\left[\lambda_1\omega_o t - \omega_o\left(t_{o1} - \tau_o\right)\right]\right.$$

$$\left. + A_2\left(t - t_b\right)\cos\left[\lambda_2\omega_o t - \omega_o\left(t_{o2} - \tau_o\right)\right]\right\}^2 \quad (96)$$

which, upon squaring and expanding, yields

$$g_{s1,2}(t) = \frac{A_o^2\left[J_o(B)\right]^4}{8}\left\{A_1^2\left(t - t_b\right)\left(1 + \cos 2\left[\lambda_1\omega_o t - \omega_o\left(t_{o1} - \tau_o\right)\right]\right)\right.$$

$$+ A_2^2\left(t - t_b\right)\left(1 + \cos 2\left[\lambda_2\omega_o t - \omega_o\left(t_{o2} - \tau_o\right)\right]\right)$$

$$+ A_1\left(t - t_b\right) A_2\left(t - t_b\right)\left(\cos\left[\left(\lambda_1 + \lambda_2\right)\omega_o t - \omega_o\left(t_{o1} + t_{o2} - 2\tau_o\right)\right]\right.$$

$$\left.\left. + \cos\left[\left(\lambda_1 - \lambda_2\right)\omega_o t - \omega_o\left(t_{o1} - t_{o2}\right)\right]\right)\right\} \qquad (97)$$

By comparing equations (94) and (97), we obtain two new terms because of the cross product of the signals from two points. One of the new terms is the sum of the two Doppler frequencies, while the second new term is a low-frequency component from the difference of the two Doppler frequency components, i.e., assuming the two Doppler components are almost equal. Extending the analysis to the signal return from N points, the output of the square-law device becomes

$$g_{sn}(t) = \frac{A_o^2\left[J_o(B)\right]^4}{4}\left\{\sum_{i=1}^{N} A_i\left(t - t_b\right)\cos\left[\lambda_i\omega_o t - \omega_o\left(t_{oi} - \tau_o\right)\right]\right\}^2 \qquad (98)$$

from which we shall obtain

$$\frac{N(N-1)}{2}$$

cross product terms. Thus, the effect of considering a distributed target versus a point target due to the square-law device is the generation of additional cross product terms due to all points under consideration. We shall see that the low-frequency cross product terms will introduce distortion at the low-pass filter output.

Equation (97) shows that not only will terms involving the $A_i\left(t - t_b\right)$ appear but cross terms such as

$$A_i\left(t - t_b\right) A_j\left(t - t_b\right) \quad i \neq j$$

will also appear, thus introducing additional distortion terms at the square-law device output.

d. Low-Pass Filter

As discussed previously, the function of the low-pass filter (LPF) is to extract the low-frequency range modulation function A(t). Therefore, the LPF bandpass must be wide enough to allow the spectrum of figure 21 to pass through to the output terminal. Again we will assume an ideal LPF (figure 26).

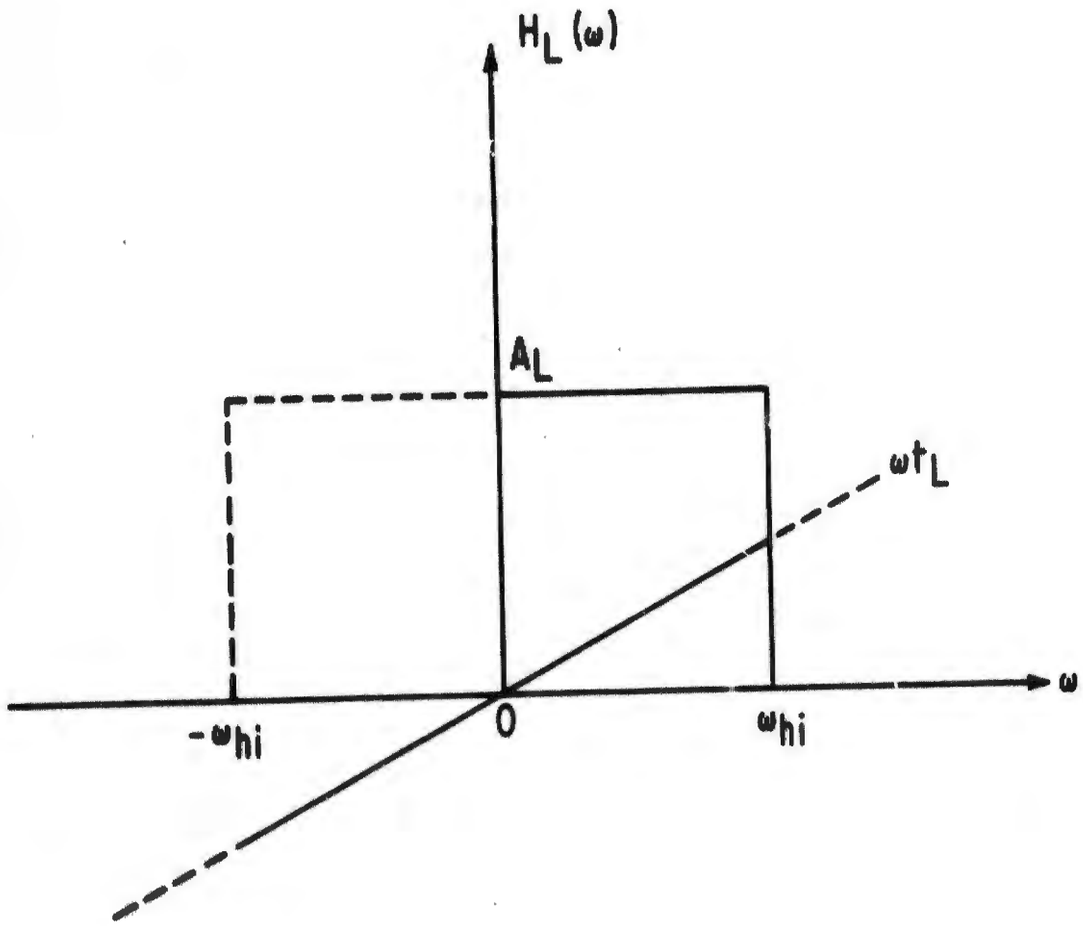

Figure 26. Low-Pass Filter Characteristic

The LPF transfer function, $H_L(\omega)$, is given by

$$H_L(\omega) = \begin{cases} A_L\, e^{-j\omega t_L} & \text{for } |\omega| < \omega_{hi} \\ 0 & \text{for } |\omega| > \omega_{hi} \end{cases} \qquad (99)$$

For a point target the LPF input is given by equation (94). Since the high-frequency component will be attenuated completely, the output becomes

$$G_L(\omega) = \left\{ \frac{A_o^2 \left[J_o(B) \right]^4}{8} A_1'(\omega) \right\} \left\{ H_L(\omega) \right\}$$

$$= \frac{A_L A_o^2 \left[J_o(B) \right]^4}{8} A_1'(\omega)\, e^{-j\omega t_L} \qquad (100)$$

where

$$A_1'(\omega) = A_1(\omega) * A_1(\omega)\, e^{-j\omega t_b} \qquad (101)$$

and * denotes convolution. By substituting equation (102) into equation (101), we obtain

$$G_L(\omega) = \frac{A_L A_o^2 \left[J_o(B) \right]^4}{8} A_1(\omega) * A_1(\omega)\, e^{-j\omega\left(t_b + t_L\right)} \qquad (102)$$

and the LPF output time function becomes

$$g_L(t) = \frac{A_L A_o^2 \left[J_o(B) \right]^2}{8} \left[A_1\left(t - t_b - t_L \right) \right]^2 \qquad (103)$$

Thus, the system output due to a point target is given by equation (103). Similarly we can find the system output from two points on the surface to be

$$g_L(t) = \frac{A_L A_o^2 \left[J_o(B)\right]^4}{8} \left\{ \left[A_1\left(t - t_b - t_L\right)\right]^2 + \left[A_2\left(t - t_b - t_L\right)\right]^2 \right.$$

$$+ A_1\left(t - t_b - t_L\right) A_2\left(t - t_b - t_L\right)$$

$$\left. \cdot \cos\left(\left(\lambda_1 - \lambda_2\right)\omega_o t - \omega_o\left[t_{o1} - t_{o2} + \left(\lambda_1 - \lambda_2\right) t_L\right]\right)\right\} \qquad (104)$$

The first two terms in equation (104) are the required terms and the third term from the nonlinear operation of the square-law device adds a distortion at the output.

The number of cross product terms from N points on the surface that appear at the system output will depend on the LPF bandwidth and the difference in Doppler frequencies, $\left(\lambda_i - \lambda_j\right)\omega_o$. Because we would like to pass the complete range function spectrum through the LPF, the bandwidth is dictated by the vehicle velocity, i.e., the greater the velocity, the greater the bandwidth must become.

5. Summary

We shall now briefly summarize the effects of velocity and an extended target on the reflected signal on a homodyne system (figure 20).

Initially, we have seen that the transmitted signal is amplitude modulated and frequency shifted by the vehicle velocity. Also, when considering an extended target, a spectrum of Doppler frequencies is generated. We have found that when analyzing the postulated homodyne system, the effect of the Doppler and A(t) spectrum spreading is to increase the required system BPF bandwidth, and the affect of square-law detection on the sum of signals returned from an extended target is to produce unwanted low-frequency components which appear as distortion at the system output. Thus, for the system postulated in this section, the effect of receiving signals from extended targets may complicate the system design considerably, especially because the system's geometry may not be accurately specified and worst-case conditions would have to be considered.

We have considered the return from a thin strip, whereas in actuality the return will be the result of a three-dimensional target (if roughness is included), and the problem of determining the exact returned signal becomes exceedingly complex. The analysis carried out in this section will give the reader at least a feel for the practical problem.

SECTION VIII

SUMMARY AND CONCLUSIONS

A method for determining the signal distortion caused by a moving antenna has been exhibited. Ideal conditions of reflecting surface and vehicle geometry were assumed. The effect of the reflected signal on an FM receiver was determined. We saw that, because of the nonlinear properties in the receiver and the signal spreading caused by a finite antenna beam width, the final decision voltage would be distorted.

Numerical results for the A(t) amplitude spectrum and velocity spreading were obtained for various geometrical conditions.

The assumption of an ideal reflecting surface has allowed us to ignore the change in radar cross section, σ, as a function of angle of incidence. The σ for a random surface may be found to vary significantly with angle of incidence. This phenomenon would cause the received amplitude to vary accordingly.

The numerical results obtained in section VI have shown that the spectrum spreading caused by the rate of increase of received amplitude is greater for higher velocities and lower terminal altitudes (although the degree of spreading was found to be small). We have also seen that the Doppler spreading due to a finite beam width depends on path angle and beamwidth. The Doppler shift could be both positive and negative for a particular geometry.

The analysis of an FM receiver in section VII showed that the final decision amplitude will be distorted due to the signal spreading caused by considering the return signal from many points on the reflecting surface. Distortion caused by range-amplitude modulation was found to be small (based on the numerical results of section VI).

Based on the results of this report, it would appear that a theoretical and experimental program based on the electromagnetic theory of propagation would be desirable in order to verify the results presented here.

APPENDIX I

A SOLUTION FOR TOTAL TRANSMISSION DELAY AND ITS EFFECT ON A TRANSMITTED SPECTRUM

In this appendix we shall show the effect of vehicle motion on a transmitted signal spectrum. The exact expression for signal delay to and from the target will first be derived, then, using Laplace transform techniques, the received spectrum will be obtained.

Consider a vehicle A (figure 27) traveling at a velocity V from the point R_o toward the reflecting plane at 0. At an altitude $R_o'(t)$ the vehicle transmits a signal which propagates at a velocity c toward the origin 0. The time that it will take the signal to arrive at 0 is

$$t' = \frac{R_o'(t)}{c} \tag{105}$$

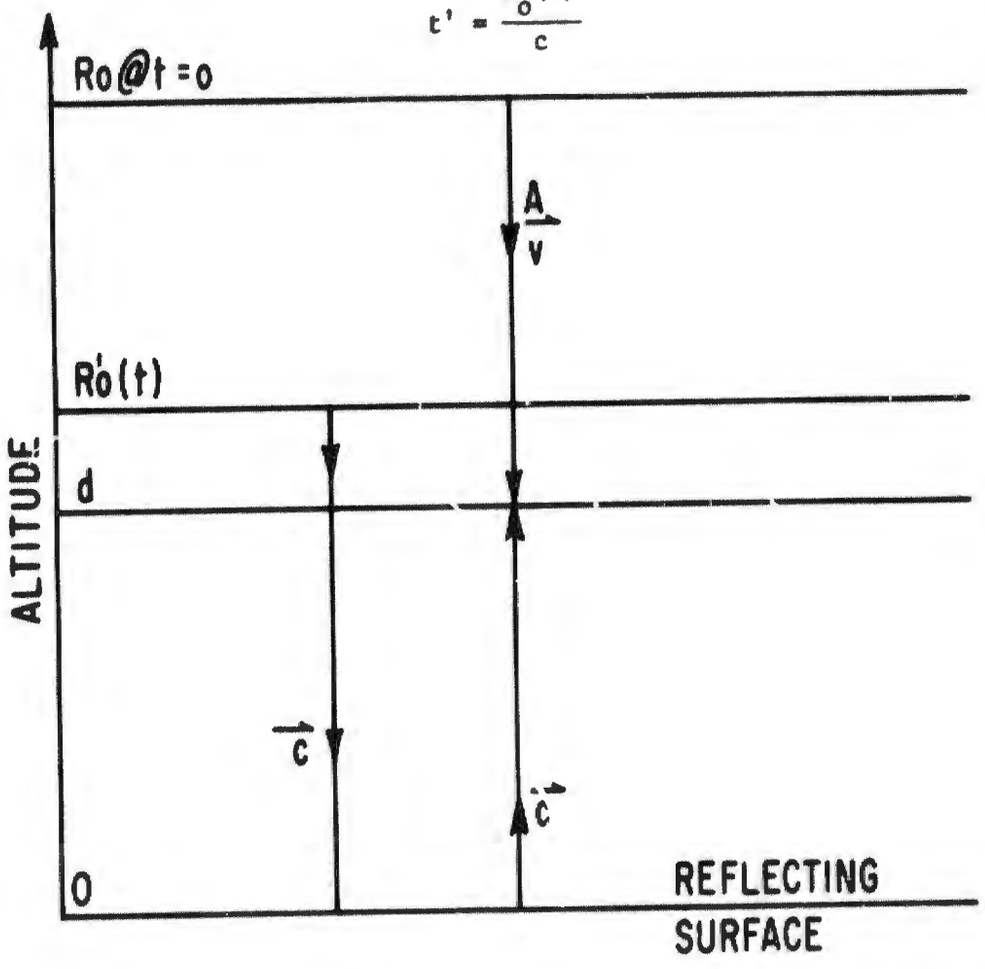

Figure 27. Geometry Used in Calculating Total Delay

The signal is then reflected from the conducting surface back to the vehicle. The problem will be to find the exact receiving point when A has continued at velocity V after having transmitted the signal.

While the signal travels toward 0, the vehicle travels a distance

$$R_o'(t)\,\frac{V}{c} \tag{106}$$

and is at the point

$$R_o'(t)\left(1 - \frac{V}{c}\right)$$

at the instant the signal is reflected from 0. The signal then travels a distance

$$d = ct'' \tag{107}$$

and the vehicle travels to the point

$$d = R_o'(t)\left(1 - \frac{V}{c}\right) - Vt'' \tag{108}$$

equating distances (equations (107) and (108)), we obtain

$$ct'' = R_o'(t)\left(1 - \frac{V}{c}\right) - Vt'' \tag{109}$$

or

$$t'' = R_o'(t)\,\frac{1 - \frac{V}{c}}{V + c} \tag{110}$$

The total time for the signal to travel from the vehicle to 0 and back is

$$t_d = t' + t'' \tag{111}$$

or from equations (105) and (110)

$$t_d = \frac{R_o'(t)}{c} + R_o'(t)\,\frac{1 - \frac{V}{c}}{V + c} \tag{112}$$

and substituting

$$R_o'(t) = R_o - Vt \tag{113}$$

into equation (112), we obtain

$$t_d = \frac{2R_o}{V + c} - \frac{2V}{V + c} t \tag{114}$$

where $t = 0$ when the vehicle is at R_o.

Therefore, if the transmitted signal is $S_t(t)$, an observer at 0 would see a delayed version of $S_t(t)$:

$$S_o(t) = S_t(t - t') \tag{115}$$

and the observer A will, after reflection, see the signal

$$S_r(t) = S_t\left(t - t_d\right) \tag{116}$$

or from equation (112)

$$S_r(t) = S_t\left(t - \frac{2R_o}{V + c} + \frac{2V}{V + c} t\right) \tag{117}$$

Rearranging equation (117), we obtain

$$S_r(t) = S_t\left[t\left(1 + \frac{2V}{V + c}\right) - \frac{2R_o}{V + c}\right] \tag{118}$$

Usually we can assume that $c >> V$ and equation (118) becomes

$$S_r(t) = S_t\left[t\left(1 + \frac{2V}{c}\right) - \frac{2R_o}{c}\right] \tag{119}$$

where $\frac{2V}{c}$ is a time compression and $\frac{2R_o}{c}$ is a time delay.

Frequency Analysis

Assuming

$$S_t(t) = 0 \quad \text{for } t < 0$$

the Laplace transorm of $S_r(t)$ is

$$\mathcal{L}\left\{S_r(t)\right\} = \int_0^\infty S_r(t)\, e^{-st}\, dt \tag{120}$$

Substituting equation (119) into equation (120), we obtain

$$\mathcal{L}\left\{S_r(t)\right\} = \int_0^\infty S_t\left[t\left(1 + \frac{2V}{c}\right) - \frac{2R_o}{c}\right] e^{-st}\, dt \tag{121}$$

Let

$$a = 1 + \frac{2V}{c}$$

$$b = \frac{2R_o}{c}$$

and

$$\tau(t) = at - b$$

then

$$d\tau = a\,dt$$

Equation (121) may now be written as

$$\mathcal{L}\left\{S_r(t)\right\} = \int_0^\infty \frac{1}{a} S_t(\tau)\, e^{-s\left[\frac{\tau(t)+b}{a}\right]}\, d\tau \tag{122}$$

or

$$\mathcal{L}\left\{S_r(t)\right\} = \frac{1}{a} e^{-s\frac{b}{a}} \int_0^\infty S_t(\tau)\, e^{-s\frac{\tau(t)}{a}}\, d\tau \tag{123}$$

which becomes

$$\mathcal{L}\left\{S_r(t)\right\} = F_r(s) = \frac{1}{a} e^{-s\frac{b}{a}} F_t\left(\frac{s}{a}\right) \tag{124}$$

or in terms of $F_t(s)$

$$F_t(s) = \frac{e^{bs}}{a} F_r(as) \tag{125}$$

$$= \frac{e^{\frac{2R_o}{c}s}}{1 + \frac{2V}{c}} F_r\left[s\left(1 + \frac{2V}{c}\right)\right] \tag{126}$$

The amplitude spectrum is given by

$$\left| F_t(\omega) \right| = \left| \frac{F_r\left[\omega\left(1 + \frac{2V}{c}\right)\right]}{1 + \frac{2V}{c}} \right| \tag{127}$$

and the phase spectrum by

$$\Phi(\omega) = \frac{2R_o}{c}\omega \tag{128}$$

Assuming a transmitted amplitude spectrum of the form (figure 3)

$$\left|F_t(\omega)\right| = 1, \ \omega_{Lo} \leq \omega \leq \omega_{hi} \tag{129}$$

with zero phase, the received signal will then be

$$F_r(\omega) = \frac{1}{1 + \frac{2V}{c}} \tag{130}$$

with phase

$$\left|\phi(\omega)\right| = \frac{2R_o}{c}\ \omega \tag{131}$$

The amplitude and phase spectrums are shown in figures 28 and 29. The amplitude spectrum is seen to be reduced and stretched by the factor $1 + \frac{2V}{c}$, i.e., the higher frequencies are shifted by a greater amount than the lower frequencies. The phase shift increases linearly with frequency.

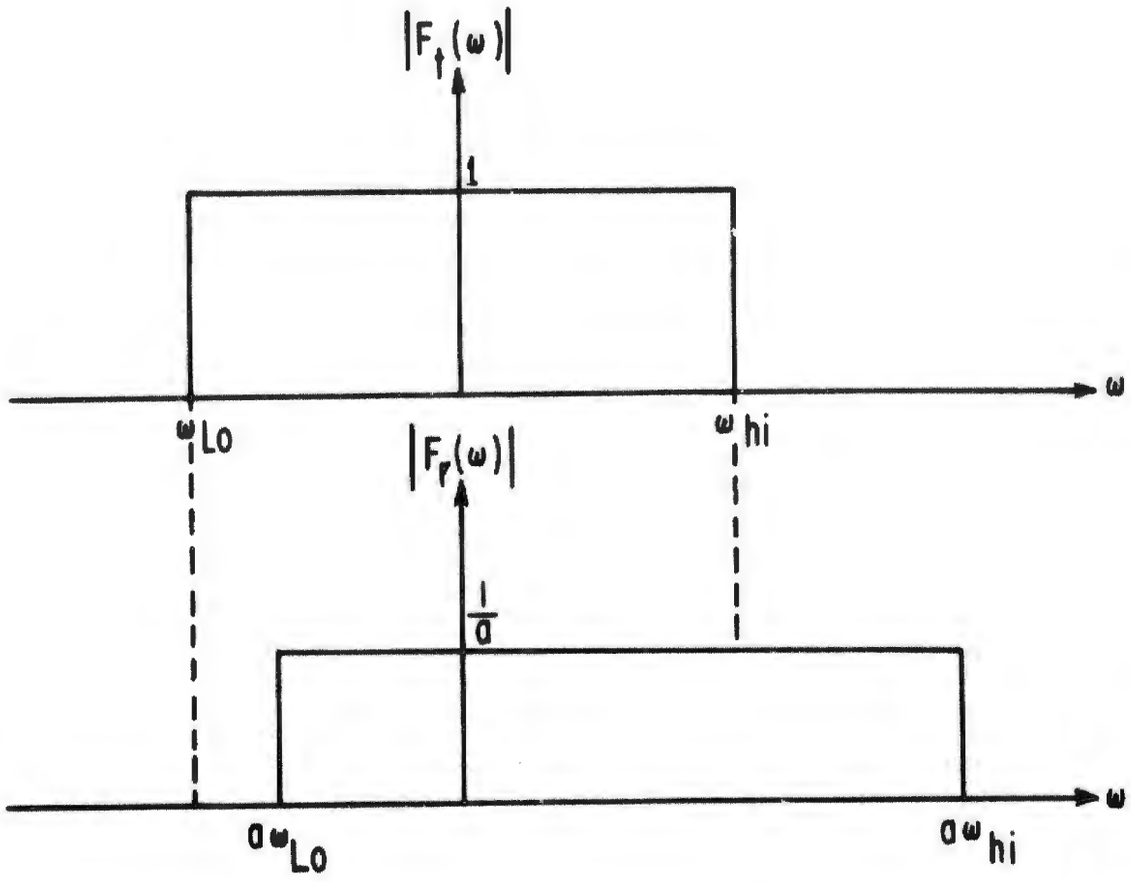

Figure 28. Amplitude Spectrum for Transmitted and received Signals

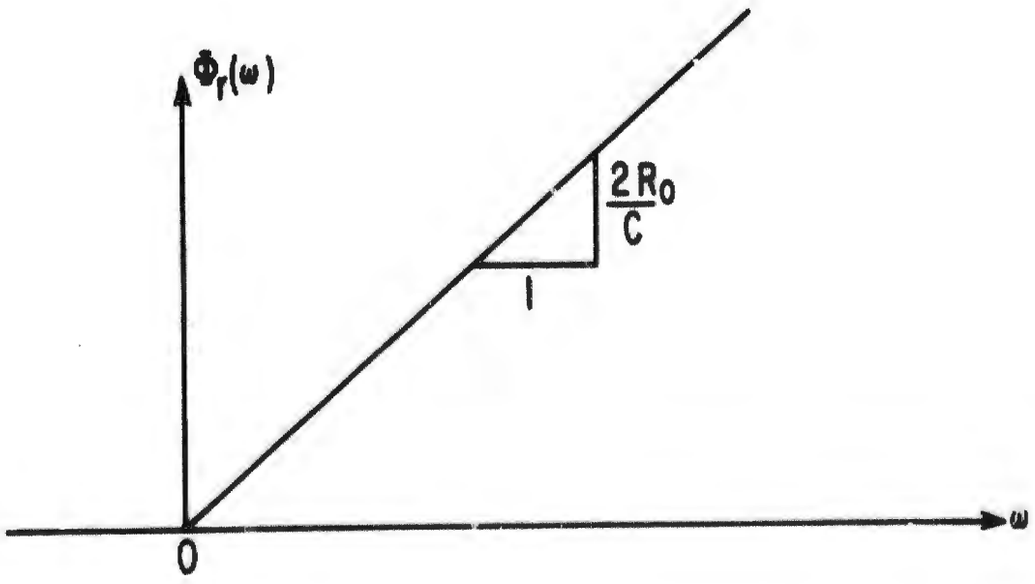

Figure 29. Received Signal Phase Spectrum

APPENDIX II

GEOMETRICAL INTERPRETATION OF THE DOPPLER FREQUENCY

The Doppler frequency shift is a phenomenon associated with the relative velocity of the transmitter with respect to the target. A surface of constant velocity vectors can be associated with the antenna motion. This surface of constant velocity vectors forms a cone with the antenna as the vertex and the flight path the axis. The constant velocity cone is a right circular cone. Of particular interest are the lines of constant Doppler formed by the intersection of the velocity cone and the reflecting surface. These intersections will, in general, be conical sections, i.e., ellipses, parabolas, and hyperbolas. The particular conic that is formed will depend on various critical angles such as flight path angle, antenna beam width and angle of incidence.

In this study we have assumed that the antenna beam is oriented such that the straight line between the antenna and the flat reflecting surface is perpendicular to the surface and forms the axis of the conical radiation pattern. For this derivation we shall also assume that the antenna is stationary.

The geometry is shown in figure 30. The antenna path is directed from point V to point I. The beamwidth is 2β and the flight path angle is γ. The origin of the coordinate system is chosen on the surface at the point 0 directly beneath the antenna.

Let the point $P(\rho,\theta)$ be any point within the illuminated area on the surface for

$$0 \leq \rho \leq \rho_{max} \tag{132}$$

and

$$-\frac{\pi}{2} \leq \theta \leq +\frac{\pi}{2} \tag{133}$$

These limits for ρ and θ are due to the symmetry about the Y - Z plane (the flight path is in the Y - Z plane).

The angle of incidence δ will be limited by

$$\delta_{min} \leq \delta \leq \frac{\pi}{2} \tag{134}$$

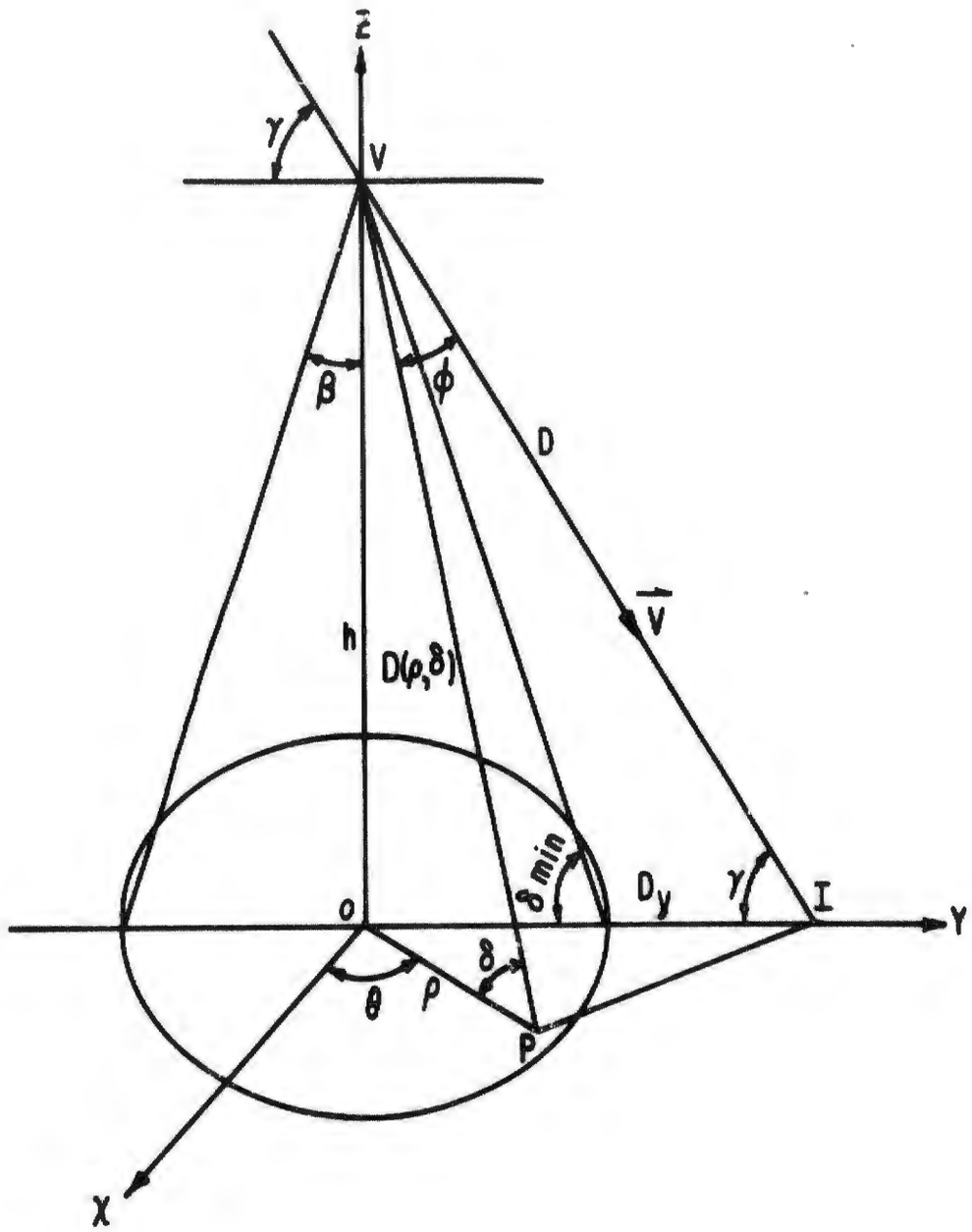

Figure 30. Antenna Geometry for Computing Velocity Components

while ρ is the distance from the origin to any point $P(\rho,\theta)$ in the illuminated area. The angle ϕ will serve to define the velocity cone angle and is a function of θ, ρ, and δ.

It is clear that the velocity component of the antenna velocity, relative to the reflecting surface, in the direction $P(\rho,\theta)$ is required to determine the limits of Doppler within the illuminated area.

In general, at a particular altitude h, the velocity at any point P will be a function of ρ, θ, and δ.

The velocity, $V(\rho,\theta,\delta)$, may now be written in terms of $\phi(\rho,\theta,\delta)$ as

$$V(\rho,\theta,\delta) = |V| \cos \left[\phi(\rho,\theta,\delta)\right] \tag{135}$$

From figure 30 the line segment PI can be found by using the law of cosines for triangle PIO.

$$\overline{PI}^2 = \rho^2 + D^2 - 2\rho D_y \cos (90° - \theta) \tag{136}$$

PI may also be found by writing the law of cosines for triangle PIV.

$$\overline{PI}^2 = \left[D(\rho,\delta)\right]^2 + D^2 - 2D(\rho,\delta)\, D \cos \left[\phi(\rho,\theta,\delta)\right] \tag{137}$$

setting these two equations equal to each other, we have

$$\rho^2 + D_y^2 - 2\rho D_y \cos (90° - \theta)$$

$$= \left[D(\rho,\delta)\right]^2 + D^2 - 2D(\rho,\delta)\, D \cos \left[\phi(\rho,\theta,\delta)\right] \tag{138}$$

From figure 30

$$D_y = h \cot \gamma \text{ (a constant)} \tag{139}$$

$$D = h \csc \gamma \text{ (a constant)} \tag{140}$$

$$D(\rho,\delta) = \rho \sec \delta \text{ (a variable)} \tag{141}$$

we also have that

$$\cos (90° - \theta) = \sin \theta$$

combining equations (138), (139), (140), (141), (142), we obtain

$$\cos \phi(\rho,\theta,\delta) = (h + \rho \cot \gamma \sin \theta) \frac{\sin \gamma}{\sqrt{h^2 + \rho^2}}$$

This equation does not depend on δ directly and

$$\cos \phi(\rho,\theta) = \frac{\sin \gamma}{\sqrt{h^2 + \rho^2}} (h + \rho \cot \gamma \sin \theta) \tag{143}$$

or rather than equation (143), we may write

$$\cos \phi(\theta,\delta) = \sin \gamma \sin \delta + \cos \gamma \cos \delta \sin \theta \tag{144}$$

From equations (135), (143), and (144), we obtain

$$V(\rho,\theta) = |V| \left(\frac{h}{\sqrt{h^2 + \rho^2}} \sin \gamma + \frac{\rho}{\sqrt{h^2 + \rho^2}} \cos \gamma \sin \theta \right) \tag{145}$$

or in terms of θ and δ

$$V(\theta,\delta) = |V| \ (\sin \gamma \sin \delta + \cos \gamma \cos \delta \sin \theta) \tag{146}$$

From equation (146), it can be seen that for a vertical flight path ($\gamma = \pi/2$)

$$V(\theta,\delta) = |V| \sin \delta$$

which depends only on δ and the lines of constant velocity become circles. For $0 < \gamma < \pi/2$, the lines of constant velocity on the surface will be in the form of ellipses (figure 31).

From equations (145) and (146), the velocity to any point on the surface may be found. Equation (146) shows that in general the velocity to any point depends on the angle θ, the angle of incidence δ, and the flight path angle γ.

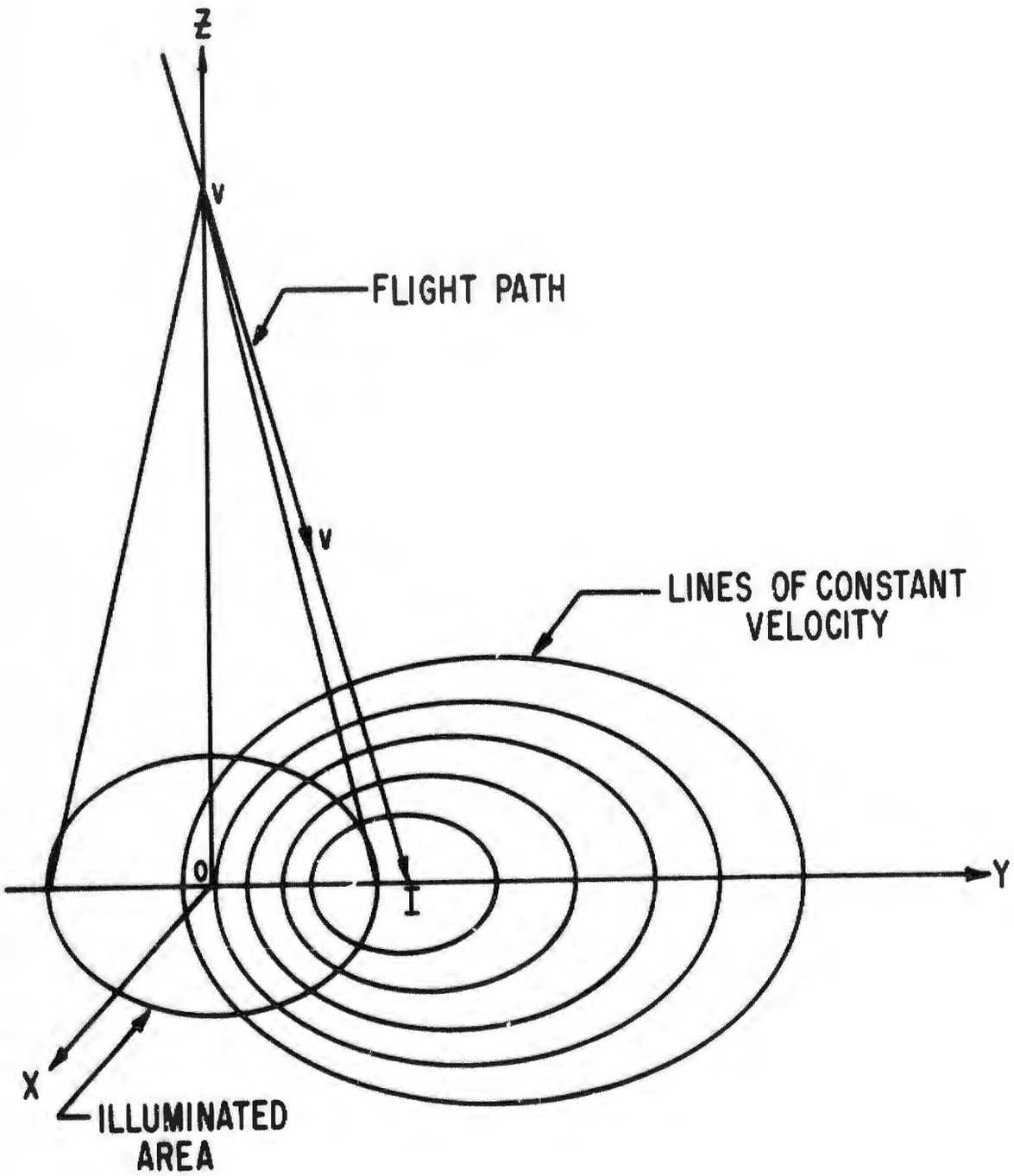

Figure 31. Lines of Constant Velocity for Nonvertical Flight Path

The Doppler frequency shift at any point is then given by

$$f_d(\theta,\delta) = \frac{2V(\theta,\delta)}{c} f_c \qquad (147)$$

where c is the velocity of propagation of the signal and f_c is the carrier frequency. Equation (147) may be written as

$$f_d\left(\theta_i,\delta_i\right) = \frac{2V\left(\theta_i,\delta_i\right)}{c} f_c$$

for the Doppler shift due to the velocity component to the i^{th} point on the reflecting surface.

This page intentionally left blank.

APPENDIX III

DETERMINATION OF THE BALANCED MIXER DIFFERENCE FREQUENCY COMPONENTS

In this appendix we will determine the balanced mixer (BM) difference frequency output. After expansion, Eq. (70) may be written as

$$S_r(t) = A(t)\, J_o(B) \cos\left[\left(\omega_o+\lambda\omega_o\right) t - \omega_o t_o\right]$$

$$+ A(t)\sum_{n=1}^{\infty} J_{2n}(B)\left\{\cos\left[\left(\omega_o+\lambda\omega_o+2n\omega_m+2n\lambda\omega_m\right) t-\omega_o t_o-2n\omega_m t_o\right]\right.$$

$$\left. + \cos\left[\left(\omega_o+\lambda\omega_o-2n\omega_m-2n\lambda\omega_m\right) t - \omega_o t_o+2n\omega_m t_o\right]\right\}$$

$$+ A(t)\sum_{n=0}^{\infty} J_{2n+1}(B)\left\{\cos\left(\left[\omega_o+\lambda\omega_o+(2n+1)\ \omega_m+(2n+1)\ \lambda\omega_m\right] t-\omega_o t_o-(2n+1)\omega_m t_o\right)\right.$$

$$\left. - \cos\left(\left[\omega_o+\lambda\omega_o-(2n+1)\ \omega_m-(2n+1)\ \lambda\omega_m\right] t-\omega_o t_o+(2n+1)\omega_m t_o\right)\right\} \qquad (149)$$

and Eq (71) is written as

$$S_d(t) = J_o(B)\cos\left(\omega_o t-\omega_o\tau_o\right)$$

$$+\sum_{n=1}^{\infty} J_{2n}(B)\left\{\cos\left[\left(\omega_o+2n\omega_m\right) t-\omega_o\tau_o - 2n\omega_m\tau_o\right]\right.$$

$$\left. + \cos\left[\left(\omega_o-2n\omega_m\right) t-\omega_o\tau_o -(2n+1)\ \omega_m\tau_o\right]\right\}$$

$$+\sum_{n=0}^{\infty} J_{2n+1}(B)\left\{\cos\left(\left[\omega_o+(2n+1)\omega_m\right] t-\omega_o\tau_o-(2n+1)\omega_m\tau_o\right)\right.$$

$$\left. - \cos\left(\left[\omega_o-(2n+1)\omega_m\right] t-\omega_o\tau_o+(2n+1)\omega_m\tau_o\right)\right\} \qquad (150)$$

Multiplying Eq (149) and Eq (150) we obtain

$$
\begin{aligned}
G_{BM}(t) = {} & A(t)J_o(B)J_o(B) \cos\left(\omega_o t-\omega_o\tau_o\right) \cos\left[\left(\omega_o+\lambda\omega_o\right) t-\omega_o t_o\right] \\
& + A(t)J_o(B)\sum_{n=1}^{\infty} J_{2n}(B) \cos\left[\left(\omega_o+\lambda\omega_o\right) t-\omega_o t_o\right] \cos\left[\left(\omega_o+2n\omega_m\right) t-\omega_o\tau_o-2n\omega_m\tau_o\right] \\
& + A(t)J_o(B)\sum_{n=1}^{\infty} J_{2n}(B) \cos\left[\left(\omega_o+\lambda\omega_o\right) t-\omega_o t_o\right] \cos\left[\left(\omega_o-2n\omega_m\right) t-\omega_o\tau_o+2n\omega_m\tau_o\right] \\
& + A(t)J_o(B)\sum_{n=0}^{\infty} J_{2n+1}(B) \cos\left[\left(\omega_o+\lambda\omega_o\right) t-\omega_o t_o\right] \cos\left(\left[\omega_o+(2n+1)\omega_m\right] t-\omega_o\tau_o-(2n+1)\omega_m\tau_o\right) \\
& - A(t)J_o(B)\sum_{n=0}^{\infty} J_{2n+1}(B) \cos\left[\left(\omega_o+\lambda\omega_o\right) t-\omega_o t_o\right] \cos\left(\left[\omega_o-(2n+1)\omega_m\right] t-\omega_o\tau_o+(2n+1)\omega_m\tau_o\right) \\
& + A(t)J_o(B)\sum_{n=1}^{\infty} J_{2n}(B) \cos\left(\omega_o t-\omega_o\tau_o\right) \cos\left[\left(\omega_o+\lambda\omega_o+2n\omega_m+2n\lambda\omega_m\right) t-\omega_o t_o-2n\omega_m t_o\right] \\
& + A(t)\sum_{n=1}^{\infty}\sum_{k=1}^{\infty} J_{2n}(B)J_{2k}(B) \cos\left[\left(\omega_o+\lambda\omega_o+2n\omega_m+2n\lambda\omega_m\right) t-\omega_o t_o-2n\omega_m t_o\right] \\
& \cos\left[\left(\omega_o+2k\omega_m\right) t-\omega_o\tau_o-2k\omega_m\tau_o\right] \\
& + A(t)\sum_{n=1}^{\infty}\sum_{k=1}^{\infty} J_{2n}(B)J_{2k}(B) \cos\left[\left(\omega_o+\lambda\omega_o+2n\omega_m+2n\lambda\omega_m\right) t-\omega_o t_o-2n\omega_m t_o\right] \\
& \cos\left[\left(\omega_o-2k\omega_m\right) t-\omega_o\tau_o+2k\omega_m\tau_o\right] \\
& + A(t)\sum_{n=1}^{\infty}\sum_{k=0}^{\infty} J_{2n}(B)J_{2k+1}(B) \cos\left[\left(\omega_o+\lambda\omega_o+2n\omega_m+2n\lambda\omega_m\right) t-\omega_o t_o-2n\omega_m t_o\right] \\
& \cos\left(\left[\omega_o+(2k+1)\omega_m\right] t-\omega_o\tau_o-(2k+1)\omega_m\tau_o\right)
\end{aligned}
$$

$$+ A(t) \sum_{n=1}^{\infty} \sum_{k=0}^{\infty} J_{2n}(B) J_{2k+1}(B) \cos \left[\left(\omega_o + \lambda\omega_o + 2n\omega_m + 2n\lambda\omega_m \right) t - \omega_o t_o - 2n\omega_m t_o \right]$$

$$\cos \left(\left[\omega_o + (2k+1)\omega_m \right] t - \omega_o \tau_o - (2k+1)\omega_m \tau_o \right)$$

$$- A(t) \sum_{n=1}^{\infty} \sum_{k=0}^{\infty} J_{2n}(B) J_{2k+1}(B) \cos \left[\left(\omega_o + \lambda\omega_o + 2n\omega_m + 2n\lambda\omega_m \right) t - \omega_o t_o - 2n\omega_m t_o \right]$$

$$\cos \left(\left[\omega_o - (2k+1)\omega_m \right] t - \omega_o \tau_o + (2k+1)\omega_m \tau_o \right)$$

$$+ A(t) J_o(B) \sum_{n=1}^{\infty} J_{2n}(B) \cos \left[\left(\omega_o + \lambda\omega_o - 2n\omega_m - 2n\lambda\omega_m \right) t - \omega_o t_o + 2n\omega_m t_o \right] \cos \left(\omega_o t - \omega_o \tau_o \right)$$

$$+ A(t) \sum_{n=1}^{\infty} \sum_{k=1}^{\infty} J_{2n}(B) J_{2k}(B) \cos \left[\left(\omega_o + \lambda\omega_o - 2n\omega_m - 2n\lambda\omega_m \right) t - \omega_o t_o + 2n\omega_m t_o \right]$$

$$\cos \left[\left(\omega_o + 2k\omega_m \right) t - \omega_o \tau_o - 2k\omega_m \tau_o \right]$$

$$+ A(t) \sum_{n=1}^{\infty} \sum_{k=1}^{\infty} J_{2n}(B) J_{2k}(B) \cos \left[\left(\omega_o + \lambda\omega_o - 2n\omega_m - 2n\lambda\omega_m \right) t - \omega_o t_o + 2n\omega_m t_o \right]$$

$$\cos \left[\left(\omega_o - 2k\omega_m \right) t - \omega_o \tau_o + 2k\omega_m \tau_o \right]$$

$$+ A(t) \sum_{n=1}^{\infty} \sum_{k=0}^{\infty} J_{2n}(B) J_{2k+1}(B) \cos \left[\left(\omega_o + \lambda\omega_o - 2n\omega_m - 2n\lambda\omega_m \right) t - \omega_o t_o + 2n\omega_m t_o \right]$$

$$\cos \left(\left[\omega_o + (2k+1)\omega_m \right] t - \omega_o \tau_o - (2k+1)\omega_m \tau_o \right)$$

$$- A(t) \sum_{n=1}^{\infty} \sum_{k=0}^{\infty} J_{2n}(B) J_{2k+1}(B) \cos \left[\left(\omega_o + \lambda\omega_o - 2n\omega_m - 2n\lambda\omega_m \right) t - \omega_o t_o + 2n\omega_m t_o \right]$$

$$\cos \left(\left[\omega_o - (2k+1)\omega_m \right] t - \omega_o \tau_o + (2k+1)\omega_m \tau_o \right)$$

$$+A(t)J_o(B)\sum_{n=o}^{\infty} J_{2n+1}(B)\cos\left[\left(\omega_o+\lambda\omega_o+(2n+1)\omega_m+(2n+1)\lambda\omega_m\right)t-\omega_o t_o-(2n+1)\omega_m t_o\right]$$

$$\cos\left(\omega_o t-\omega_o\tau_o\right)$$

$$+A(t)\sum_{n=0}^{\infty}\sum_{k=1}^{\infty} J_{2n+1}(B)J_{2k}(B)\cos\left(\left[\omega_o+\lambda\omega_o+(2n+1)\omega_m+(2n+1)\lambda\omega_m\right]t-\omega_o t_o-(2n+1)\omega_m t_o\right)$$

$$\cos\left[\left(\omega_o+2k\omega_m\right)t-\omega_o\tau_o-2k\omega_m\tau_o\right]$$

$$+A(t)\sum_{n=0}^{\infty}\sum_{k=1}^{\infty} J_{2n+1}(B)\,J_{2k}(B)\cos\left(\left[\omega_o+\lambda\omega_o+(2n+1)\omega_m+(2n+1)\lambda\omega_m\right]t-\omega_o t_o-(2n+1)\omega_m t_o\right)$$

$$\cos\left[\left(\omega_o-2k\omega_m\right)t-\omega_o\tau_o+2k\omega_m\tau_o\right]$$

$$+A(t)\sum_{n=0}^{\infty}\sum_{k=0}^{\infty} J_{2n+1}(B)J_{2k+1}(B)\cos\left(\left[\omega_o+\lambda\omega_o+(2n+1)\omega_m+(2n+1)\lambda\omega_m\right]t-\omega_o t_o-(2n+1)\omega_m t_o\right)$$

$$\cos\left(\left[\omega_o+(2k+1)\omega_m\right]t-\omega_o\tau_o-(2k+1)\omega_m\tau_o\right)$$

$$-A(t)\sum_{n=0}^{\infty}\sum_{k=0}^{\infty} J_{2n+1}(B)\,J_{2k+1}(B)\cos\left(\left[\omega_o+\lambda\omega_o+(2n+1)\omega_m+(2n+1)\lambda\omega_m\right]t-\omega_o t_o-(2n+1)\omega_m t_o\right)$$

$$\cos\left(\left[\omega_o-(2k+1)\omega_m\right]t-\omega_o\tau_o+(2k+1)\omega_m\tau_o\right)$$

$$
\begin{aligned}
&- A(t)J_o(B)\sum_{n=0}^{\infty} J_{2n+1}(B)\ \cos\left(\left[\omega_o+\lambda\omega_o-(2n+1)\omega_m-(2n+1)\lambda\omega_m\right]\ t-\omega_o t_o+(2n+1)\omega_m t_o\right)\\
&\cos\left(\omega_o t-\omega_o\tau_o\right)\\
&- A(t)\sum_{n=0}^{\infty}\sum_{k=i}^{\infty} J_{2n+1}(B)J_{2k}(B)\ \cos\left(\left[\omega_o+\lambda\omega_o-(2n+1)\omega_m-(2n+1)\lambda\omega_m\right]\ t-\omega_o t_o+(2n+1)\omega_m t_o\right)\\
&\cos\left[\left(\omega_o+2k\omega_m\right)\ t-\omega_o\tau_o-2k\omega_m\tau_o\right]\\
&- A(t)\sum_{n=0}^{\infty}\sum_{k=1}^{\infty} J_{2n+1}(B)J_{2k}(B)\ \cos\left(\left[\omega_o+\lambda\omega_o-(2n+1)\omega_m-(2n+1)\lambda\omega_m\right]\ t-\omega_o t_o+(2n+1)\omega_m t_o\right)\\
&\cos\left[\left(\omega_o-2k\omega_m\right)\ t-\omega_o\tau_o+2k\omega_m\tau_o\right]\\
&- A(t)\sum_{n=0}^{\infty}\sum_{k=0}^{\infty} J_{2n+1}(B)J_{2k+1}(B)\ \cos\left(\left[\omega_o+\lambda\omega_o-(2n+1)\omega_m-(2n+1)\lambda\omega_m\right]\ t-\omega_o t_o+(2n+1)\omega_m t_o\right)\\
&\cos\left(\left[\omega_o+(2k+1)\omega_m\right]\ t-\omega_o\tau_o-(2k+1)\omega_m\tau_o\right)\\
&+ A(t)\sum_{n=0}^{\infty}\sum_{k=0}^{\infty} J_{2n+1}(B)J_{2k+1}(B)\ \cos\left(\left[\omega_o+\lambda\omega_o-(2n+1)\omega_m-(2n+1)\lambda\omega_m\right]\ t-\omega_o t_o+(2n+1)\omega_m t_o\right)\\
&\cos\left(\left[\omega_o-(2k+1)\omega_m\right]\ t-\omega_o\tau_o+(2k+1)\omega_m\tau_o\right) \qquad (151)
\end{aligned}
$$

From Eq (151) we can now obtain the BM difference frequencies

$$g_{BM}(t)\Big|_{DIFF} = \frac{A(t)\left[J_o(B)\right]^2}{2} \cos\left(\lambda\omega_o t-\omega_o t_o+\omega_o \tau_o\right)$$

$$+ \frac{A(t)J_o(B)}{2}\sum_{n=1}^{\infty} J_{2n}(B) \cos\left[\left(\lambda\omega_o-2n\omega_m\right) t-\omega_o \left(t_o-\tau_o\right)+2n\omega_m\tau_o\right]$$

$$+ \frac{A(t)J_o(B)}{2}\sum_{n=1}^{\infty} J_{2n}(B) \cos\left[\left(\lambda\omega_o+2n\omega_m\right) t-\omega_o \left(t_o-\tau_o\right)-2n\omega_m\tau_o\right]$$

$$+ \frac{A(t)J_o(B)}{2}\sum_{n=0}^{\infty} J_{2n+1}(B) \cos\left(\left[\lambda\omega_o-(2n+1)\omega_m\right] t-\omega_o \left(t_o-\tau_o\right)+(2n+1)\omega_m\tau_o\right)$$

$$- \frac{A(t)J_o(B)}{2}\sum_{n=0}^{\infty} J_{2n+1}(B) \cos\left(\left[\lambda\omega_o+(2n+1)\omega_m\right] t-\omega_o \left(t_o-\tau_o\right)-(2n+1)\omega_m\tau_o\right)$$

$$+ \frac{A(t)J_o(B)}{2}\sum_{n=1}^{\infty} J_{2n}(B) \cos\left(\left[\lambda\omega_o+2n\omega_m(1+\lambda)\right] t-\omega_o\left(t_o-\tau_o\right) -2n\omega_m t_o\right)$$

$$+ \frac{A(t)}{2}\sum_{n=1}^{\infty}\sum_{k=1}^{\infty} J_{2n}(B)J_{2k}(B) \cos\left(\left[\lambda\omega_o+2n\omega_m(1+\lambda) -2k\omega_m\right] t-\omega_o\left(t_o-\tau_o\right)-2\omega_m\left(nt_o-k\tau_o\right)\right)$$

$$+ \frac{A(t)}{2}\sum_{n=1}^{\infty}\sum_{k=1}^{\infty} J_{2n}(B)J_{2k}(B) \cos\left(\left[\lambda\omega_o+2n\omega_m(1+\lambda)+2k\omega_m\right] t-\omega_o\left(t_o-\tau_o\right)-2\omega_m\left(nt_o+k\tau_o\right)\right)$$

$$+\frac{A(t)}{2}\sum_{n=1}^{\infty}\sum_{k=0}^{\infty} J_{2n}(B)J_{2k+1}(B)\cos\left(\left[\lambda\omega_o+2n\omega_m(1+\lambda)-(2k+1)\omega_m\right]t-\omega_o(t_o-\tau_o)-\omega_m\left[2nt_o-(2k+1)\tau_o\right]\right)$$

$$-\frac{A(t)}{2}\sum_{n=1}^{\infty}\sum_{k=0}^{\infty} J_{2n}(B)J_{2k+1}(B)\cos\left(\left[\lambda\omega_o+2n\omega_m(1+\lambda)+(2k+1)\omega_m\right]t-\omega_o(t_o-\tau_o)-\omega_m\left[2nt_o+(2k+1)\tau_o\right]\right)$$

$$+\frac{A(t)J_o(B)}{2}\sum_{n=1}^{\infty} J_{2n}(B)\cos\left(\left[\lambda\omega_o-2n\omega_m(1+\lambda)\right]t-\omega_o(t-\tau_o)+2n\omega_m t_o\right)$$

$$+\frac{A(t)}{2}\sum_{n=1}^{\infty}\sum_{k=1}^{\infty} J_{2n}(B)J_{2k}(B)\cos\left(\left[\lambda\omega_o-2n\omega_m(1+\lambda)-2k\omega_m\right]t-\omega_o(t_o-\tau_o)+2\omega_m(nt_o+k\tau_o)\right)$$

$$+\frac{A(t)}{2}\sum_{n=1}^{\infty}\sum_{k=1}^{\infty} J_{2n}(B)J_{2k}(B)\cos\left(\left[\lambda\omega_o-2n\omega_m(1+\lambda)-2k\omega_m\right]t-\omega_o(t_o-\tau_o)+2\omega_m(nt_o-k\tau_o)\right)$$

$$+\frac{A(t)}{2}\sum_{n=1}^{\infty}\sum_{k=0}^{\infty} J_{2n}(B)J_{2k+1}(B)\cos\left(\left[\lambda\omega_o-2n\omega_m(1+\lambda)-(2k+1)\omega_m\right]t-\omega_o(t_o-\tau_o)+\omega_m\left[2nt_o+(2k+1)\tau_o\right]\right)$$

$$-\frac{A(t)}{2}\sum_{n=1}^{\infty}\sum_{k=0}^{\infty} J_{2n}(B)J_{2k+1}(B)\cos\left(\left[\lambda\omega_o-2n\omega_m(1+\lambda)+(2k+1)\omega_m\right]t-\omega_o(t_o-\tau_o)+\omega_m\left[2nt_o-(2k+1)\tau_o\right]\right)$$

$$+\frac{A(t)J_o(B)}{2}\sum_{n=0}^{\infty} J_{2n+1}(B)\cos\left(\left[\lambda\omega_o+(2n+1)\omega_m(1+\lambda)\right]t-\omega_o(t_o-\tau_o)-(2n+1)\omega_m t_o\right)$$

$$+\frac{A(t)}{2}\sum_{n=0}^{\infty}\sum_{k=1}^{\infty}J_{2n+1}(B)J_{2k}(B)\cos\left(\left[\lambda\omega_o+(2n+1)\omega_m(1+\lambda)-2k\omega_m\right]t-\omega_o\left(t_o-\tau_o\right)-\omega_m\left[(2n+1)t_o-2k\tau_o\right]\right)$$

$$+\frac{A(t)}{2}\sum_{n=0}^{\infty}\sum_{k=1}^{\infty}J_{2n+1}(B)J_{2k}(B)\cos\left(\left[\lambda\omega_o+(2n+1)\omega_m(1+\lambda)+2k\omega_m\right]t-\omega_o\left(t_o-\tau_o\right)-\omega_m\left[(2n+1)t_o+2k\tau_o\right]\right)$$

$$+\frac{A(t)}{2}\sum_{n=0}^{\infty}\sum_{k=0}^{\infty}J_{2n+1}(B)J_{2k+1}(B)\cos\left(\left[\lambda\omega_o+(2n+1)\omega_m(1+\lambda)-(2k+1)\omega_m\right]t-\omega_o\left(t_o-\tau_o\right)-\omega_m\left[(2n+1)t_o-(2k+1)\tau_o\right]\right)$$

$$-\frac{A(t)}{2}\sum_{n=0}^{\infty}\sum_{k=0}^{\infty}J_{2n+1}(B)J_{2k+1}(B)\cos\left(\left[\lambda\omega_o+(2n+1)\omega_m(1+\lambda)+(2k+1)\omega_m\right]t-\omega_o\left(t_o-\tau_o\right)-\omega_o\left[(2n+1)t_o+(2k+1)\tau_o\right]\right)$$

$$-\frac{A(t)J_o(B)}{2}\sum_{n=0}^{\infty}J_{2n+1}(B)\cos\left(\left[\lambda\omega_o-(2n+1)\omega_m(1+\lambda)\right]t-\omega_o\left(t_o-\tau_o\right)+(2n+1)\omega_m t_o\right)$$

$$-\frac{A(t)}{2}\sum_{n=0}^{\infty}\sum_{k=1}^{\infty}J_{2n+1}(B)J_{2k}(B)\cos\left(\left[\lambda\omega_o-(2n+1)\omega_m(1+\lambda)-2k\omega_m\right]t-\omega_o\left(t_o-\tau_o\right)+\omega_m\left[(2n+1)t_o+2k\tau_o\right]\right)$$

$$-\frac{A(t)}{2}\sum_{n=0}^{\infty}\sum_{k=1}^{\infty}J_{2n+1}(B)J_{2k}(B)\cos\left(\left[\lambda\omega_o-(2n+1)\omega_m(1+\lambda)+2k\omega_m\right]t-\omega_o\left(t_o-\tau_o\right)+\omega_m\left[(2n+1)t_o-2k\tau_o\right]\right)$$

$$-\frac{A(t)}{2}\sum_{n=0}^{\infty}\sum_{k=0}^{\infty}J_{2n+1}(B)J_{2k+1}(B)\cos\left(\left[\lambda\omega_o-(2n+1)\omega_m(1+\lambda)-(2k+1)\omega_m\right]t-\omega_o\left(t_o-\tau_o\right)+\omega_m\left[(2n+1)t_o+(2k+1)\tau_o\right]\right)$$

$$+\frac{A(t)}{2}\sum_{n=0}^{\infty}\sum_{k=0}^{\infty}J_{2n+1}(B)J_{2k+1}(B)\cos\left(\left[\lambda\omega_o-(2n+1)\omega_m(1+\lambda)+(2k+1)\omega_m\right]t-\omega_o\left(t_o-\tau_o\right)+\omega_m\left[(2n+1)t_o-(2k+1)\tau_o\right]\right)$$

(152)

REFERENCES

1. Ament, W. S., Toward a Theory of Reflection by a Rough Surface, Proceedings of the I.R.E., Vol 41, 1953.

2. Davies, H., The Reflection of Electromagnetic Waves from a Rough Surface, Proceedings of the I.E.E., (London), Part IV, Vol 101, August 1954.

3. Moore, R. K., Williams, C. S., Jr., Radar Terrain Return at Near Vertical Incidence, Proceedings of the I.R.E., Vol 45, February 1957.

4. Beckmann, P., Spizzichino, A., The Scattering of Electromagnetic Waves from Rough Surfaces, The MacMillian Co, New York, 1963.

5. Moore, R. K., Resolution of Vertical Incidence Radar Return into Random and Specular Components, Sandia Corp. Tech. Memo, SCR-7, February 1958.

6. Kerr, D. E., Ed., Propagation of Short Radio Waves, Vol 13, No. 3, October 1955.

7. Dike, S. H., Radar Pulse Return from Extended Targets, Sandia Corp. Tech. Memo, SCR 2647 (TR).

8. Kraus, J. D., Antennas, McGraw-Hill Book Co, New York, 1950.

9. Papoulis, A., The Fourier Integral and Its Applications, McGraw-Hill, Inc., New York, 1962.

UNCLASSIFIED

Security Classification

DOCUMENT CONTROL DATA - R & D

(Security classification of title, body of abstract and indexing annotation must be entered when the overall report is classified)

1. ORIGINATING ACTIVITY (Corporate author)	2a. REPORT SECURITY CLASSIFICATION
Air Force Weapons Laboratory (WLDE) Kirtland Air Force Base, New Mexico 87117	UNCLASSIFIED
	2b. GROUP

3. REPORT TITLE

AN ANALYSIS OF TRANSMITTED SIGNAL DISTORTION RESULTING FROM ANTENNA TO REFLECTING SURFACE VELOCITY

4. DESCRIPTIVE NOTES (Type of report and inclusive dates)

September 1966-February 1967

5. AUTHOR(S) (First name, middle initial, last name)

J. Philip Castillo

6. REPORT DATE	7a. TOTAL NO. OF PAGES	7b. NO. OF REFS
May 1968	100	9

8a. CONTRACT OR GRANT NO.	9a. ORIGINATOR'S REPORT NUMBER(S)
b. PROJECT NO. 5791	AFWL-TR-67-147
c. Task No. 30	9b. OTHER REPORT NO(S) (Any other numbers that may be assigned this report)
d.	

10. DISTRIBUTION STATEMENT This document is subject to special export controls and each transmittal to foreign nationals or foreign governments may be made only with prior approval of AFWL (WLDE), Kirtland AFB, NM, 87117. Distribution is limited because of the technology discussed in the report.

11. SUPPLEMENTARY NOTES	12. SPONSORING MILITARY ACTIVITY
	AFWL (WLDE) Kirtland AFB, NM 87117

13. ABSTRACT (Distribution Limitation Statement No. 2)

Distortion of transmitted signals caused by Doppler frequency spreading and amplitude modulation is a consequence of the relative velocity between the transmitter and a reflecting surface. General equations yielding velocity components to any point in the illuminated area on the surface, received power as a function of time, and generalized effects of vehicle motion on the transmitted frequency spectrum are derived. The Fourier spectrum of the range modulation function is calculated using computer techniques. With this, the spectral spreading of the transmitted signal due to rate of change of range is obtained. A specific transmitting-receiving system is analyzed. The system transmits a frequency-modulated continuous-wave (FM-CW) signal. The receiver consists of a balanced mixer, a band-pass filter, a square-law device, and a low-pass filter. The analysis of the system begins with the signal received from a single point reflector and is extended to signals received from many points simultaneously. This particular system is selected because it allows a unique analysis, in that the functional design would be dependent on the amount of signal distortion as defined in this research. A summary of the analysis is given, together with recommendations of topics for further study in the area of analysis of signals returned from various terrains.

DD FORM 1 NOV 65 1473

UNCLASSIFIED

Security Classification

14. KEY WORDS	LINK A		LINK B		LINK C	
	ROLE	WT	ROLE	WT	ROLE	WT
Doppler						
Altimeter						
Velocity distortion						
Signal processing						
Range modulation						
Terrain radar return						